6mer seed toxicity in tumor suppressive microRNAs

Quan Q. Gao[1,6], William E. Putzbach[1,6], Andrea E. Murmann[1], Siquan Chen[2], Aishe A. Sarshad[3], Johannes M. Peter[4], Elizabeth T. Bartom[5], Markus Hafner[3], and Marcus E. Peter[1,5]

[1]Department of Medicine/Division Hematology/Oncology and [5]Department of Biochemistry and Molecular Genetics, Northwestern University, Chicago, IL 60611, USA, [2]Cellular Screening Center, Institute for Genomics & Systems Biology, The University of Chicago, Chicago, IL 60637, USA, [3]Laboratory of Muscle Stem Cells and Gene Regulation, NIAMS, NIH, Bethesda, MD 20892, USA, [4]DigiPen Institute of Technology, Redmond, WA 98052, USA,

[6] Authors share first authorship

Corresponding author: Marcus E. Peter, E-mail: m-peter@northwestern.edu, phone: 312-503-1291; FAX: 312-503-0189.

Keywords: DISE, RNAi, miRNAs, strand selection, toxicity, evolution

SUMMARY

Many small interfering (si)RNAs are toxic to cancer cells through a 6mer seed sequence (position 2-7 of the guide strand). Here we performed a siRNA screen with all 4096 6mer seeds revealing a preference for guanine in positions 1 and 2 and a high overall G or C content in the seed of the most toxic siRNAs for four tested human and mouse cell lines. Toxicity of these siRNAs stems from targeting survival genes with C-rich 3'UTRs. The master tumor suppressor miRNA miR-34a-5p is toxic through such a G-rich 6mer seed and is upregulated in cells subjected to genotoxic stress. An analysis of all mature miRNAs suggests that during evolution most miRNAs evolved to avoid guanine at the 5' end of the 6mer seed sequence of the guide strand. In contrast, for certain tumor suppressive miRNAs the guide strand contains a G-rich toxic 6mer seed, presumably to eliminate cancer cells.

INTRODUCTION

RNA interference (RNAi) is a form of post-transcriptional regulation exerted by 19-21 nt long double stranded RNAs that negatively regulate gene expression at the mRNA level. RNAi-active guide RNAs can come from endogenous siRNAs and micro(mi)RNAs. For a miRNA, the RNAi pathway begins in the nucleus with transcription of a primary miRNA precursor (pri-miRNA) [1]. Pri-miRNAs are first processed by the Drosha/DGCR8 microprocessor complex into pre-miRNAs [2], which are then exported from the nucleus to the cytoplasm by Exportin 5 [3]. Once in the cytoplasm, Dicer processes them further [4, 5] and these mature dsRNA duplexes are then loaded into Argonaute (Ago) proteins to form the RNA-induced silencing complex (RISC) [6]. The sense/passenger strand is ejected/degraded, while the guide strand remains associated with the RISC [7]. Depending on the degree of complementarity between the guide strand and its target, the outcome of RNAi can either be target degradation - most often achieved by siRNAs with full complementarity to their target mRNA [8] - or miRNA-like cleavage-independent silencing, mediated by deadenylation/degradation or translational repression [9]. The latter mechanism can be initiated with as little as six nucleotide base-pairing between a guide RNA's so-called seed sequence (positions 2 to 7) and fully complementary seed matches in the target RNA [10, 11]. This seed-based targeting most often occurs in the 3'UTR of a target mRNA [12, 13].

A number of miRNAs function either as tumor suppressors or as oncogenes [14]. Their cancer specific activities are usually explained by their identified targets, being oncogenes or tumor suppressors, respectively [14]. Examples of targets of tumor-suppressive miRNAs are the oncogenes Bcl-2 for miR-15/16 [15] and c-Myc for miR-34a [16]. While many miRNAs have been reported to have both tumor suppressive and oncogenic activities depending on the cancer context, examples for widely established tumor promoting miRNAs are miR-221/222, miR-21, miR-155, and members of the miR-17~92 cluster, or its paralogues miR-106b~25 and miR-106a~363 [17, 18]. In contrast, two of the major tumor suppressive miRNA families are miR-15/16 and the p53 regulated miR-34a/c and miR-34b [19].

We recently discovered that many si- and shRNAs can kill all tested cancer cell lines through RNAi by targeting the 3'UTRs of critical survival genes [20]. We called this mechanism DISE (for death induced by survival gene elimination). Cancer cells have difficulty developing resistance to this mechanism both *in vitro* and when treated *in vivo* [21]. We reported that a 6mer seed sequence in the toxic siRNAs is sufficient for effective killing [20]. We have now performed a strand specific siRNA screen with a library of individual siRNAs representing all 4096 possible 6mer seed sequences in a neutral RNA duplex. This screen, while based on siRNA biochemistry was not designed to identify targets that are degraded through siRNA mediated slicing activity but to identify toxicity caused by moderately targeting hundreds of genes required for cell survival in a mechanism similar to miRNA-induced silencing.

We report that the most toxic 6mer seeds are G-rich with a G enrichment towards the 5' end targeting survival genes with a high C content in their 3'UTR in a miRNA-like manner. Many tumor suppressive miRNAs such as miR-34a-5p but none of the established oncogenic miRNAs contain G-rich 6mer seeds and most of miR-34a-5p's toxicity comes from its 6mer seed sequence. Mature miRNAs from older and more conserved miRNAs contain less toxic seeds. We demonstrate that for most miRNAs the more abundant mature form corresponds to the arm that contains the less toxic seed. In contrast, for major tumor suppressive miRNAs, the mature miRNA is derived from the arm that harbors the more toxic seed. Our data allow us to conclude that while most miRNAs have evolved to avoid targeting survival and housekeeping genes, certain tumor suppressive miRNAs function to kill cancer cells through a toxic G-rich 6mer seed targeting the 3'UTR of survival genes.

RESULTS

Identifying the most toxic 6mer seeds

To test whether certain 6mer seeds present in the guide strand of a siRNA affect cancer cell survival, we recently designed a neutral 19mer oligonucleotide scaffold with two nucleotide 3' overhangs, and we demonstrated that modifying a siRNA strand at positions 1 and 2 by 2'-O-methylation (OMe) completely blocks its loading into the RISC [22]. Different 6mer sequences can be inserted at positions 2-7 of the guide strand with the designated passenger strand modified by OMe (two red Xs in **Fig. 1a**). Transfection efficiency and conditions were optimized for each cell line used. To determine the general rules of seed-based toxicity, we individually transfected 4096 siRNAs with all possible 6mer seed sequences in this 19mer scaffold into two human, HeyA8 (ovarian cancer) and H460 (lung cancer), and two mouse cell lines M565 (liver cancer) and 3LL (lung cancer). This allowed us to rank all 4096 6mer seeds according to their toxicity (**Fig. 1b**, **Supplementary Data File 1,** and **6merdb.org**). The congruence between the results of the two human cell lines and the two human and two mouse cell lines was quite high (r=0.68 and 0.73, respectively, **Fig. 1c**) suggesting that many siRNAs were toxic through a mechanism independent of cancer origin and

species. Toxicity was caused by the different 6mer seeds in the *guide* strand. A siRNA duplex highly toxic to all cell lines (#2733, HeyA8 cell viability = 1.4%) strongly inhibited cell growth and reduced cell viability of HeyA8 cells only when the passenger strand but not when the guide strand was modified by the OMe modification. Toxicity was completely blocked when the guide strand was modified (**Supplementary Figure 1a**). The toxicity was due to RNAi as knockdown of AGO2 abolished the toxicity of two of the most toxic siRNAs (**Supplementary Figure 1b**).

We previously reported that the CD95 ligand (CD95L) coding region (CDS) is enriched in sequences that when converted into si- or shRNAs are toxic to cancer cells [20] and most recently that the CD95L mRNA itself is toxic to cells [23]. We now report a substantial correlation between the most toxic CD95L-derived shRNAs and the toxicity of their predicted 6mer seed (**Fig. 1d**) suggesting the CD95L-derived si/shRNAs kill cancer cells through 6mer seed toxicity. Consistent with this assumption we found that the 6mer seeds of 4 previously tested siRNAs derived from CD95L [24] in this screen were about as toxic as the full length siRNAs, with siL3^{Seed} being the most toxic followed by siL2^{Seed} and less or no toxicity associated with siL4^{Seed} and siL1^{Seed} (**Fig. 1b, Fig. 1c**). Our recent analysis suggested that the toxic si/shRNAs act like artificial miRNAs by targeting the 3'UTR of mRNAs [20].

6mer seeds enriched in G at the 5'end are most toxic

We noticed that the 6mer seeds in siL3 and siL2 have a higher G content than the ones in siL4 and siL1 (**Fig. 1b**). By analyzing the screen results of all four cell lines (**Supplementary Figure 2**), we found that a high G content of the seed correlated better with toxicity than a high C content. Almost no toxicity was found with seeds with a high A content. To test the effect of nucleotide content on toxicity directly, we retested the 19 seed duplexes with the highest content (>80%) for each of the four nucleotides in the four cell lines (**Fig. 2**). The reanalysis also allowed us to determine the reproducibility of the results obtained in the large screens (which for technical reasons had to be performed in three sets). All data on the three cell lines were highly reproducible especially for the most toxic seeds (**Supplementary Figure 3a**). When the data on the four cell lines were compared, it became apparent that in all cell lines, the G-rich seeds were by far the most toxic followed by the C-rich, U-rich, and A-rich seeds (**Fig. 2a**). This indicates it is mostly the G content that determines toxicity.

Most genome-wide siRNA libraries designed to study functions of individual genes are highly underrepresented in G and C to increase RNAi specificity [25] (**Supplementary Figure 3b**, left panel). In contrast, our complete set of 6mer seed duplexes exhibits no nucleotide composition bias, allowing us to test the contributions of all four nucleotides in each of the 6 seed positions (**Supplementary Figure 3b**, right panel). To determine the nucleotide content of the most toxic seeds, we determined the frequency of each nucleotide at each of the 6 positions of either the 200 most or 200 least toxic seed duplexes for each of the

two human and the two mouse cells (**Fig. 2b**, **Supplementary Data File 1**). We found that a high G content towards the 5' end of the seed and a C in position 6 was most toxic (**Fig. 2b** and **Supplementary Figure 3c**). In contrast, non-toxic seeds were A and U-rich especially when positioned at the 5' end. The rules of toxicity that emerged are almost identical between human and mouse, suggesting evolutionary conservation. This can also be explored at 6merdb.org.

Toxic siRNAs target C-rich housekeeping genes

We previously showed that si- and shRNAs are toxic through 6mer seed toxicity preferentially targeting hundreds of genes critical for cell survival [20]. We had developed a Toxicity Index (TI), a simple tool to predict the most toxic seeds based on the ratio of putative seed match occurrences in the 3'UTR of set of survival genes (SGs) versus a set of genes not required for cell survival (nonSGs). We now compared the TI with our experimentally determined 6mer seed toxicity in the four cell lines screened (**Supplementary Figure 4**) and found a significant correlation between these two types of analyses, further supporting the mechanism of toxicity. Knowing that seed sequences rich in G are most toxic suggested the targeted genes carry C-rich seed matches in their 3'UTR. To be most stringent, we used a list of the 20 6mer seeds that were most toxic to both HeyA8 and H460 cells (**Supplementary Data File 2**). The G richness towards the 5' end of the 6mers in these toxic seeds and the 5' A/U richness of the nontoxic seeds was even more pronounced than in the top/bottom 200 most toxic seeds (**Fig. 3a**). We scored for the occurrence of seed matches to the 20 seeds in each group in the 3'UTR, the CDS and the 5'UTR of a set of 938 critical SGs similar to one recently described [20] and an expression-matched set of 938 nonSGs. We found a significantly higher count ratio of toxic versus nontoxic seed matches in the 3'UTR of SGs when compared to nonSGs (**Fig. 3b**, right panel). Consistent with a miRNA-like function no such enrichment was found when the CDS was analyzed (**Fig. 3b**, center panel). An inverse ratio of sequences complementary to the 6mer seeds of unknown significance was found in the 5'UTR (**Fig. 3b**, left panel). This result was very similar when we scored for seed matches to the 100 seeds most toxic and least toxic to both human cell lines (**Supplementary Figure 5a**). An enrichment of the exact seed matches in 3'UTRs was consistent with the overall higher C content of 3'UTRs of SGs when compared to nonSGs (different peak maxima in **Fig. 3c**). A metaplot analysis of the 500 bases upstream and downstream of the translational start and stop site of all human genes showed that as expected the 3'UTR was enriched in A and U (**Fig. 3d**, top). Interestingly, SGs had a lower A/U content in a region ~150-500 bases into the 3'UTR than expression matched nonSGs (**Fig. 3d**, blue horizontal bar, bottom two panels). To determine where survival genes are being targeted by toxic seed containing siRNAs we again performed a metaplot analysis - this time plotting the locations of seed matches to the 20 6mer seeds that were most and least toxic to both human cell lines (**Fig. 3e**, an analysis with the 100 most/least toxic seeds is provided in **Supplementary Figure 5b**). When analyzing all human coding genes we found the

reverse complements of the most toxic seeds to be highly enriched at the beginning of the 3'UTR whereas the reverse complements of the least toxic seeds were underrepresented in this region (**Fig. 3e**, top). This effect was not due to a much higher G/C or lower A/U content in this region (**Fig. 3d**, top). A comparison of the location of these seed matches in the SGs and in expression matched nonSGs confirmed this general trend, however, two differences between SGs and nonSGs became apparent: 1) nonSGs have more nontoxic seed matches ~150-500 bases into the 3'UTR (**Fig. 3e**, bottom, blue horizontal bar) maybe due to the higher A/U content of this region (**Fig. 3d**, two bottom panels). 2) SGs contain a small stretch at positions 42-65 into the 3'UTR (**Fig. 3e** and **Supplementary Figure 5b**, center, green horizontal bar) that is enriched in seed matches for the most toxic seeds. This region in SGs seems to be a preferential target site for siRNAs carrying toxic G-rich seed sequences.

miR-34a-5p kills cancer cells through its toxic 6mer seed

The toxic siRNAs kill cancer cells through 6mer seed toxicity by a mechanism reminiscent of the function of miRNAs. To test whether actual miRNAs could kill cancer cells with the help of toxic 6mer seeds, we analyzed the seed toxicity determined in our screen for all known ~2600 mature miRNAs expressed as either the 3p or 5p arm (**6merdb.org**). While none of the 6mer seeds present in the predominant arm (guide strand) of the most oncogenic miRNAs (miR-221/222, miR-21, miR-155, the miR-17~92, miR-106b~25, and miR-106a~36 clusters) were toxic (reduced viability >50%, stippled line in **Fig. 4a**), two of the major tumor suppressive miRNA families, miR-15/16 and p53 regulated miR-34a/c and miR-34b contained toxic seeds in the guide strand (**Fig. 4a**). This suggested these two families were killing cancer cells through toxic 6mer seeds. Interestingly, two other major tumor suppressive families, let-7 and miR-200, did not contain toxic G-rich seeds in their guide strand, suggesting they may be tumor suppressive through other mechanisms, such as inducing and maintaining cell differentiation [26].

When transfecting the pre-miRs of miR-34a-5p, miR-15a-5p, and let-7a-5p into HeyA8 cells, the potency of these three miRNAs to reduce cell growth mimicked the toxicity of their 6mer seed containing siRNAs (**Fig. 4b** and **4a**). This suggested that a large part of their toxicity comes from the composition of the seed position 2-7. The most toxic seed in a major tumor suppressive miRNA was present in miR-34a-5p/34c-5p, a master regulator of tumor suppression [27]. We directly compared the toxicity of pre-miR-34a-5p and its toxic seed in the neutral scaffold with blocked passenger strand (si34a-5p^{Seed}) in the same assays (**Fig. 4c**). Strikingly, the toxicity evoked by these two RNA species (assessed by growth inhibition and DNA fragmentation) was similar. Cells showed the typical morphology we found in cells dying from toxic siRNAs (**Fig. 4d**) [20, 24, 28]. To determine the contribution of the 6mer seed sequence of miR-34a-5p to its toxicity and the mode of cell death, we performed a RNA-Seq analysis on HeyA8 cells transfected with either miR-34a-5p or si34a-5p^{Seed} (**Fig. 5a**, top) (**Supplementary Data File 3**). The vast majority of genes were significantly

up- and downregulated by both RNA duplexes (**Fig. 5a**, bottom). While miR-34a-5p targeted a subset of genes not affected by miR-34a-5p^{Seed}, the majority of differentially expressed genes (>78%) were downregulated >1.5 fold by both the premiR and the 6mer seed duplex (**Fig. 5b**, left). A Sylamer analysis is a unbiased approach allowing to identify which seed matches are enriched in the 3'UTRs of downregulated genes from RNAseq data [29]. In this analysis both duplexes caused similar and highly effective downregulation of the mRNAs that carry a 6mer seed match (**Fig. 5c**). When the Sylamer analysis was performed with either 7mer or 8mer seeds, enrichment of seed matches was much less significant (**Supplementary Figure 6a**) suggesting that most of the targeting by both RNAs only required a 6mer seed.

Consistent with this activity, targeting by both RNA duplexes resulted in a very similar reduction of survival genes (**Fig. 5d**). The genes downregulated by both the premiR and the 6mer seed construct were highly enriched in genes involved in regulation of cell cycle, cell division, DNA repair, and nucleosome assembly (**Fig. 5b**, right). These GO terms were very similar to the ones we found enriched in downregulated genes in cells dying after transfection with CD95R/L-derived si/shRNAs containing toxic 6mer seeds [20]. In contrast, no such GO terms were found enriched when the same analysis was performed with the upregulated genes as control (**Supplementary Figure 6b**). While both miR-34-5p and si34a-5p^{Seed} caused the most significant downregulation of genes carrying 8mers in their 3'UTR (**Supplementary Figure 6c**), only the most highly downregulated genes that carry the shared 6mer seed match were grouped in a number of GO terms that are consistent with 6mer seed toxicity as previously reported [20] and barely any GO terms were shared among genes that contained 7 or 8mer seed matches (**Supplementary Figure 6d**). All these data suggest that miR-34a-5p kills cancer cells using its toxic 6mer seed. While optimal miRNA targeting requires at least a 7mer seed interaction and also involves nucleotides at positions 13-16 of the miRNA [30], the cell death inducing activity of this tumor suppressive miRNA may only require the 6mer seed.

Toxic 6mer seed toxicity is shaping the miRNA repertoire

Toxic 6mer seeds may be a driving force in miRNA evolution, whereby toxic seed sequences are either selected against - because they contribute to cell toxicity - or are preserved to operate as tumor suppressors. Based on the composition of toxic 6mer seeds and the enrichment of corresponding seed matches in survival genes, we could now ask whether and when miRNAs that contain toxic G-rich sequences in positions 2-7 of their seeds evolved. When comparing all mature miRNA arms annotated in TargetScan Human 7, we noticed that miRNAs in highly conserved miRNA seed families contained 6mer seed sequences that were much less toxic in our screen than seeds in poorly conserved miRNAs (**Fig. 6a,** left panel and **Supplementary Figure 7a**). Weakly conserved miRNA seed families would be expected to be younger in evolutionary age than highly conserved ones. Consistent with this assumption we found that the 6mer seeds of younger miRNAs (<10 million years old) were more likely to be toxic to cells than the ones of older miRNAs (>800 million

years old) [31] (**Fig. 6a**, right panel and **Supplementary Figure 7b**). Most importantly, when comparing miRNAs of different ages, it became apparent that seeds of miRNAs over the last 800 million years were gradually depleted of G beginning at the 5' end and eventually also affecting positions 3-5 until the oldest ones, where A and U had replaced G as the most abundant nucleotide in all six positions (**Fig. 6b**). These analyses indicated that most highly conserved miRNAs avoid G in potentially toxic seed positions. Interestingly, the most toxic seed sequences were found in miRtrons (**Fig. 6c** and **Supplementary Figure 7c**), miRNAs that are derived by splicing short introns [32]. Across all mature miRtrons we found G to be the most abundant nucleotide in position 2-7 (**Supplementary Figure 7d**) and this region was also near the region in all miRtrons predicted to contain the 6mer sequences with the highest toxicity (**Supplementary Figure 7e**).

miRNAs are expressed as pre-miRs and usually only one major species of mature miRNA (either the 5p or the 3p arm) is significantly expressed in cells produced from one of the two strands of the premiR stem [33]. Consistent with the assumption that cells cannot tolerate toxic 6mer seeds, we now examined across 780 miRNAs which have been shown to give rise to both a 3p and a 5p arm whether the more highly expressed arm contains a seed of lower toxicity than the lesser expressed arm (**Fig. 6d**). We ranked the miRNAs according to the ratio of the 6mer seed toxicity associated with the guide arm to the lesser-expressed arm (**Supplementary Data File 4**). When we labeled the major tumor suppressive and oncogenic miRNAs, we noticed the highly expressed arm of most of the oncogenic miRNAs contained a 6mer seed that was not toxic in our screen (**Fig. 6d**, blue dots). In contrast, for most of the tumor suppressive miRNAs, the dominant arm contained a seed much more toxic than the lesser arm (**Fig. 6d**, red dots). The overall difference in ratio between the two groups of miRNAs was highly significant. A more detailed analysis of these data revealed that the three oncogenic miRNAs with the highest ratio in toxicity between their arms, miR-363, miR-92a-2, and miR-25, were almost exclusively expressed as the non-toxic 3p form (**Fig. 6e**, top). In contrast, the dominant arm of the three tumor suppressive miRNAs, miR-34a, miR-34c, and miR-449b contained the most toxic seed sequence (**Fig. 6e**, bottom). Interestingly, miR-449b has the same seed sequence as miR-34a and has been suggested to act as a backup miRNA for miR-34a [34]. These data are consistent with most tumor suppressive miRNAs using 6mer seed toxicity to kill cancer cells and suggest that this mechanism developed over hundreds of millions of years.

Genotoxic drugs upregulate toxic 6mer seed containing miRNAs

Our data showing that miR-34a-5p contains a toxic 6mer seed, along with miR-34a being upregulated after genotoxic stress [19], led us to wonder whether miR-34a-5p would contribute to cell death induced by genotoxic drugs and whether this type of cell death shared similarities to the death observed in cells dying from toxic 6mer seed containing si/shRNAs. This would be consistent with the observation that many

genotoxic drugs induce multiple cell death pathways [35, 36, 37, 38, 39]. To compare cell death induced by different genotoxic agents with that of toxic si/shRNAs, we treated the p53 wild-type ovarian cancer cell line HeyA8 with doxorubicin (Doxo), carboplatin (Carbo), or etoposide (Eto) and performed a RNA-Seq analysis. Drug concentrations were chosen so that after 80 hrs, treatment would slow down cell growth and induce signs of stress without major cell death occurring to capture changes that could be causing cell death rather than being the result of it (**Supplementary Figure 8a**). The morphological changes in the cells treated with the drugs were very similar to the ones seen in cells treated with si/shRNAs (**Supplementary Figure 8b**), and similar to reported morphologies of cells treated with genotoxic drugs [40, 41].

The ranked lists of downregulated RNAs isolated from HeyA8 cells treated with the three drugs were subjected to a gene set enrichment analysis (GSEA) to determine whether survival genes were enriched in the downregulated genes (**Supplementary Figure 9a**). There was strong enrichment of downregulated survival genes towards the top of the ranked list. 102 of the survival genes were downregulated in cells treated with any of the three drugs (**Supplementary Figure 9b**). In a DAVID gene ontology analysis, these genes were strongly enriched in clusters involved in chromosome segregation, DNA replication, cell cycle regulation, and mitosis, typical for 6mer seed toxicity induced cell death (**Supplementary Data File 5**). We quantified 30 of the 102 survival genes in HeyA8 cells treated with Doxo at different time points using an arrayed quantitative PCR (**Supplementary Figure 9c**). 24 of the 30 genes' mRNAs were significantly downregulated as early as 7 hours after treatment with no further reduction beyond 15 hrs after treatment, suggesting that their repression was the cause of cell death rather than a consequence. A Metascape analysis of all RNA-Seq data of downregulated RNAs in response to the toxic siL3, si34a-5p^{Seed}, miR-34a-5p, and the three genotoxic drugs suggested a common mode of action (**Supplementary Figure 9d**). The GO clusters that were most significantly downregulated in all data sets were again related to DNA repair, cell cycle, and mitosis as described before for cells undergoing DISE [24].

To test whether treatment of cells with genotoxic drugs results in loading the RISC with toxic miRNAs, HeyA8 cells were treated with Doxo for 0, 20, 40 and 80 hrs and all 4 Ago proteins were pulled down using a GW182 peptide [42]. Interestingly, while the amount of AGO2 pulled down was the same at all time points, the amount of bound miRNA-sized RNAs substantially increased with longer treatment times (**Fig. 7a**). This was most likely the result of an overall increase in total small RNAs in the treated cells (**Fig. 7b**). Alternatively, this could also be a result of cells dividing more slowly and a stable RISC. miR-34a/b/c-5p bound to Ago proteins were upregulated at all time points (**Supplementary Figure 10a**). To determine the contribution of miR-34a-5p and other miRNAs to the toxicity seen in cells exposed to the genotoxic drugs, we treated *Drosha* k.o. cells - devoid of most canonical miRNAs [43] - with the three genotoxic drugs (**Supplementary Figure 11a**). These cells were hypersensitive to the toxicity induced by any of the three drugs. We attributed this response to the absence of most canonical miRNAs that protect cells from toxic

RNAi active sequences [20]. This result also suggested involvement of small RNAs that do not require Drosha for processing. As expected, the composition of small RNAs bound to Ago proteins dramatically varied between wild-type and *Drosha* k.o. cells (**Fig. 7c**). In the absence of most canonical miRNAs, miR-320a-3p, which was previously shown not to require Drosha for its biogenesis [43], represented more than 86% of all Ago-bound miRNAs. Similar to HeyA8 cells (see **Supplementary Figure 10a**), Ago-bound miR-34a-5p was upregulated in wild-type but not in *Drosha* k.o. HCT116 cells upon Doxo treatment (**Supplementary Figure 10b**, right). Interestingly, the average 6mer seed toxicity of all Ago-bound miRNAs >1.5 fold upregulated in HCT116 wt cells was significantly higher than the ones >1.5 fold downregulated in cells treated with Doxo (**Fig. 7d**, left). While in the *Drosha* k.o. cells, a number of nontoxic miRNAs were downregulated, the only miRNA that was upregulated in the RISC (1.49 fold) was miR-320a-3p (**Fig. 7d**, right). However, upon closer inspection it became clear that this form of miR-320a-3p was shortened by two nucleotides at the 5' end. This resulted in the shift of the 6mer seed into a G-rich sequence (**Fig. 7d**, right), converting a moderately toxic miRNA (average viability = 49.2%) into a highly toxic one (average viability = 9.3%). To test this predicted increase in toxicity experimentally, we transfected HeyA8 cells with either the authentic pre-miR-320a-3p or a miR-320a-3p^{Seed} duplex that corresponded to the shifted Ago-bound miR-320a-3p sequence (miR-320a-3p^{Ago}) (**Fig. 7e**). While pre-miR-320a-3p was not toxic, miR-320a-3p^{Ago} completely blocked the growth of the cells. Toxicity of miR-320a-3p^{Ago} was established in the four human and mouse cell lines (**Fig. 7f**). These data suggested that in the absence of other miRNAs that could kill cells through 6mer seed toxicity, miR-320a-3p (and possibly other small RNAs) may represent an alternative mechanism that ensures that genotoxic stressors can kill cells with defective miRNA processing often observed in cancer [44, 45]. To test whether the 6mer seed toxicity exerted by miR-34a would be synergistic with the toxicity caused by the three genotoxic drugs, we treated HeyA8 cells with a low dose (1 nM) of miR-34a with low doses of either Doxo, Eto or Carbo (**Supplementary Figure 11b**). No synergism was observed consistent with the assumption that genotoxic drugs are killing the cells at least in part through the use of toxic RNAi active RNAs. In summary, our data suggest that certain tumor suppressive miRNAs, such as miR-34a-5p and miR-320a-3p exert their tumor suppressive activities by carrying toxic 6mer seed sequences that can kill cancer cells by targeting survival genes in C-rich regions close to the start of their 3'UTR. This activity may contribute to the cell death induced by genotoxic drugs.

DISCUSSION

We previously discovered a fundamental cell type- and species-independent form of toxicity that is evoked by the 6mer seed sequence in si-/shRNAs that function similar to miRNAs [20]. We have now performed an siRNA screen that effectively tested the miRNA activities of all 4096 different 6mer seed sequences.

Performing the screen in four cell lines (two human and two mouse) ensured that the results were relatively independent of species or cell type specific transcriptomes. The screen has discovered the rules underlying this seed toxicity and allows prediction of the 6mer seed toxicity for any siRNA, shRNA, miRNA with a known 6mer seed (https://6merdb.org).

Based on this screen, the toxicity of a number of tumor suppressive miRNAs could be predicted solely on the basis of their 6mer seed sequences. The enrichment of G in the first 2-3 positions of the most toxic seeds is consistent with the way Ago proteins scan mRNAs as targets. This involves mainly the first few nucleotides (positions 1-3) of the seed [46]. miR-34a-5p contains two Gs in positions 1 and 2 of its 6mer seed. While miR-34a-5p is considered a master tumor suppressive miRNA, no single target has been identified to be responsible for this activity. Over 700 targets implicated in cancer cell proliferation, survival, and resistance to therapy have been described [16]. Our data now suggest that miR-34a-5p uses 6mer seed toxicity to target hundreds of housekeeping genes. They provide the means to rationally design new artificial miRNAs as anti-cancer reagents that attack networks of survival genes. In humans, miR-34a is highly expressed in many tissues. Consistent with our data that delivering siRNAs with toxic 6mer seeds to mice are not toxic to normal cells [21] miR-34a exhibits low toxicity to normal cells *in vitro* and *in vivo* [47]. miR-34a (MRX34) became the first miRNA to be tested in a phase I clinical trial of unresectable primary liver cancer [27, 48]. The study was recently terminated and reported immune-related adverse effects in several individuals. It was suggested that these adverse effects may have been caused by either a reaction to the liposome-based carrier or the use of double-stranded RNA [16]. In addition, they may be due to an undesired gene modulation by miR-34a itself defined by sequences outside the 6mer seed [16]. Our data suggest that miR-34a exerts toxicity mostly through the 6mer seed of its 5p arm and that its 700 known targets may be part of the network of survival genes that are targeted. The comparison of the RNA-Seq data of cells treated with either miR-34a-5p or si34-5p^{Seed} now allows to determine whether these two activities can be separated.

Our data provide evidence that genotoxic drugs kill cancer cells, at least in part, by triggering the toxic 6mer seed mechanism. Exposure of cancer cells to such drugs resulted in upregulation of tumor suppressive miRNAs, most prominently of the p53 regulated miR-34 family [19]. While one report demonstrated that inhibiting miR-34a rendered cancer cells more resistant to cell death induced by genotoxic stress [49], another one found no effect of knocking out miR-34a on the sensitivity of HCT116 or MCF-7 cells to Doxo [50]. This mechanism may be highly redundant and may involve many miRNAs. Our analysis of Ago-bound miRNAs in *Drosha* k.o. cells suggest that in the absence of miR-34a, the noncanonical miR-320a-3p which was recently also found to be p53 regulated [51] may act as a backup miRNA that can still respond to genotoxic stress in case the amounts of other miRNAs are reduced, for instance in cases of mutations in miRNA biogenesis associated genes frequently found in human cancers [44]. In addition, recent data suggest that other

toxic small RNAs can also be taken up by the RISC and negatively regulate cell growth through their toxic 6mer seed [23].

It was shown before that miRNAs overall avoid seed sequences that target the 3'UTR of survival/housekeeping genes [52, 53]. Survival genes therefore are depleted in seed matches for the most abundant miRNAs in a cell. That also means 3'UTRs of survival genes must be enriched in sequences not targeted by the seeds present in most miRNAs. Our combined data now suggest it is these sequences that toxic siRNAs and tumor suppressive miRNAs with toxic 6mer seeds are targeting. Our analyses also suggest that most miRNAs have evolved over the last 800 million years by gradually depleting G in their seeds beginning at the 5' end. In addition, the most abundant miRNAs have evolved to use the arm with the lower 6mer seed toxicity as the active guide strand, presumably to avoid killing cells. Only in a minority of tumor-suppressive miRNAs does the dominant guide strand contain a toxic seed. By ranking miRNAs according to whether they express the arm with the seed of higher toxicity, it is now possible to identify novel tumor suppressive miRNAs (see 6merdb.org).

In summary, we have determined the rules of RNAi targeting by toxic 6mer seeds. These rules allowed us to predict with some confidence which si/shRNAs or miRNAs have the potential to kill cells through their toxic 6mer seed. Toxic miRNAs seem to be involved in killing cancer cells in response to genotoxic drugs. Toxic 6mer seeds are present in a number of tumor-suppressive miRNAs that can kill cancer cells. Our data allow new insights into the evolution of miRNAs and provide evidence that 6mer seed toxicity is shaping the miRNA repertoire. In addition, they now allow to develop super toxic artificial miRNAs for the treatment of cancer.

METHODS

Reagents, cell lines and antibodies

HeyA8 (RRID:CVCL_8878) and H460 (ATCC HTB-177) cells were cultured in RPMI1640 medium (Cellgro Cat#10-040) supplemented with 10% FBS (Sigma Cat#14009C) and 1% L-Glutamine (Corning Cat#25-005). 3LL cells (RRID:CVCL_5653) were cultured in DMEM medium (Gibco Cat#12430054) supplemented with 10% FBS and 1% L-Glutamine. Mouse hepatocellular carcinoma cells M565 were from a spontaneous formed liver cancer in a male mouse carrying a floxed Fas allele [54] and cultured in DMEM/F12 (Gibco Cat#11330) supplemented with 10% FBS, 1% L-Glutamine and ITS (Corning #25-800-CR).

HCT116 parental (Cat#HC19023, RRID:CVCL_0291) and the *Drosha* k.o. clone (clone #40, Cat#HC19020) were purchased from Korean Collection for Type Cultures (KCTC). Both HCT116 cell lines were cultured in McCoy's 5A medium (ATCC, Cat#30-2007) supplemented with 10% FBS and 1% L-Glutamine. All cell lines were authenticated by STR profiling. Anti-Argonaute-2 antibody (cat#ab186733, 1:1200) was purchased from Abcam, anti-β-actin antibody from Santa Cruz (#sc-47778, 1:5000), and secondary antibody

for Western blot was Goat anti-rabbit, IgG-HRP from Southern Biotech (#SB-4030-05, 1:5000). Etoposide (Cat#BML-GR307-0100) was purchased from Enzo Life Sciences, propidium iodide (#P4864) doxorubicin (Cat#D1515) and carboplatin (Cat#C2538) were from Sigma-Aldrich.

siRNA screens and cell viability assay

To design the non-toxic siRNA backbone used in the 4096 screen, the siNT2 sequence was used as a starting point and four positions in the center of siNT2 were replaced with the complementary nucleotides in order to remove any identity between the backbone siRNA and the toxic siL3 while retaining the same GC content. Two 2'-O-methylation groups were added to positions 1 and 2 of the passenger strand to prevent loading into the RISC. The 6mer seed region (position 2-7 on the guide strand) was then replaced with one of the 4096 possible seeds. Transfection efficiency was optimized for each of the four cell lines individually. RNA duplexes were first diluted with Opti-MEM to make 30 µl solution of 10 nM as final concentration in a 384 - well plate by Multidrop Combi. Lipofectamine RNAiMAX (Invitrogen) was diluted in Opti-MEM (6 µl lipid + 994 µl of Opti-MEM for HeyA8, 15.2 µl lipid + 984.8 µl of Opti-MEM for M565, 9.3 µl of lipid + 990.7 µl of Opti-MEM for 3LL, and 7.3 µl of lipid + 993.7 µl of Opti-MEM for H460). After incubating at room temperature for 5-10 min, 30 µl of the diluted lipid was dispensed into each well of the plate that contains RNA duplexes. The mixture was pipetted up and down three times by PerkinElmer EP3, incubated at room temperature for at least 20 min, and then, the mixture was mixed again by PerkinElmer EP3. 15 µl of the mixture was then transferred into wells of three new plates (triplicates) using the PerkinElmer EP3. 50 µl cell suspension containing 320 HeyA8 or 820 M565 or 150 3LL or 420 H460 cells was then added to each well containing the duplex and lipid mix, which results in a final volume of 65 µl. Plates were left at room temperature for 30 min and then moved to a 37^{o}C incubator. 96 hours post transfection, cell viability was assayed using CellTiter - Glo (Promega) quantifying cellular ATP content. 35 µl medium was removed from each well, and 30 µl CellTiter - Glo cell viability reagent was added. The plates were shaken for 5 min and incubated at room temperature for 15 min. Luminescence was then read on the BioTek Synergy Neo2. The 4096 6mer seed containing duplexes were screened in three sets for each cell line. Each set was comprised of five 384 well plates. A number of control siRNAs of known toxicity (including siNT1 and siL3) was added to each plate to compare reproducibility. All samples were set up in triplicate (on three different plates = 15 plates/set). The data in the HeyA8, H460 and M565 screens were normalized to lipid only on each plate. The 3LL screen which showed some drift between the sets was normalized to the average viability of the cells to siNT1 correcting the variability between sets.

Transfection with short oligonucleotides

For IncuCyte experiments, HeyA8 cells were plated in 50 µl antibiotic free medium in a 96 well plate at 1000 cells/well, and 50 µl transfection mix with 0.1 µl RNAiMAX and siRNAs or miRNA precursors were added during the plating. For the AGO2 knockdown experiment, 100,000 cells/well HeyA8 cells were reverse-transfected in six-well plates with either non-targeting (Dharmacon, cat#D-001810-10-05) or an AGO2 targeting siRNA SMARTpool (Dharmacon, cat#L004639-00- 005) at 25 nM. 1 µl RNAiMAX per well was used for HeyA8 cells. Twenty-four hours after transfection with the SMARTpools, cells were reversed-transfected in a 96-well plate with siNT2, si2733, or si2733 (see **Supplementary Data File 1**) at 10 nM and monitored in the IncuCyte Zoom. To measure the knockdown efficiency, cells were lysed in RIPA buffer for western blot analysis 48 hours after transfection with the SMARTpools.

All custom siRNA oligonucleotides were ordered from integrated DNA technologies (IDT) and annealed according to the manufacturer's instructions. In addition to the 4096 siRNAs of the screen the following siRNA sequences were used:

siNT1 sense: rUrGrGrUrUrUrArCrArUrGrUrCrGrArCrUrArATT;

siNT1 antisense: rUrUrArGrUrCrGrArCrArUrGrUrArArArCrCrAAA;

siNT2 sense: rUrGrGrUrUrUrArCrArUrGrUrUrGrUrGrUrGrATT;

siNT2 antisense: rUrCrArCrArCrArArArCrArUrGrUrArArArCrCrAAA;

siL3 sense: rGrCrCrCrUrUrCrArArUrUrArCrCrCrArUrArUTT;

siL3 antisense: rArUrArUrGrGrGrUrArArUrUrGrArArGrGrGrCAA;

si-miR-34a-5p^{Seed} sense: mUmGrGrUrUrUrArCrArUrGrUrArCrUrGrCrCrATT;

si-miR-34a-5p^{Seed} antisense: rUrGrGrCrArGrUrArCrArUrGrUrArArArCrCrAAA;

miR-320a-3p^{Ago} sense: mCmGrCrCrCrUrCrUrCrArArCrCrCrArGrCrUrUTT

miR-320a-3p^{Ago} antisense: rArArGrCrUrGrGrGrUrUrGrArGrArGrGrGrCrGAA.

The following miRNA precursors and negative controls were used: hsa-miR-34a-5p (Ambion, Cat. No# PM11030), hsa-let-7a-5p (Ambion, Cat. No# PM10050), hsa-miR-320a-3p (Ambion, Cat. No# PM11621), hsa-miR-15a-5p (Ambion, Cat. No# PM10235), and miRNA precursor negative control #1 (Ambion, Cat. No# AM17110).

Western blot analysis

Protein extracts were collected by lysing cells with RIPA lysis buffer (1% SDS, 1% Triton X-100, 1% deoxycholic acid). Protein concentration was quantified using the DC Protein Assay kit (Bio-Rad, Hercules, CA). 30 µg of protein were resolved on 8–12% SDS-PAGE gels and transferred to nitrocellulose membranes (Protran, Whatman) overnight at 25 mA. Membranes were incubated with blocking buffer (5% non-fat milk in 0.1% TBS/Tween-20) for 1 hr at room temperature. Membranes were then incubated with the primary antibody diluted in blocking buffer over night at 4°C. Membranes were washed 3 times with 0.1%

TBS/Tween-20. Secondary antibodies were diluted in blocking buffer and applied to membranes for 1 hr at room temperature. After 3 more additional washes, detection was performed using the ECL reagent (Amersham Pharmacia Biotech) and visualized with the chemiluminescence imager G:BOX Chemi XT4 (Synoptics). All uncropped Western blots are shown in **Supplementary Figure 12**.

Monitoring cell growth by IncuCyte and cell death assays

Cells were seeded between 1000 and 3000 per well in a 96-well plate in triplicates. The plate was then scanned using the IncuCyte ZOOM live-cell imaging system (Essen BioScience). Images were captured every four hours using a 10× objective. Cell confluence was calculated using the IncuCyte ZOOM software (version 2015A). For treatment with genotoxic drugs HeyA8 cells were seeded at 750 cells/well and HCT116 cells were seeded at 3000 cells/well in 96-well plate and treated with one of the three genotoxic drugs (carboplatin, doxorubicin, or etoposide) at various concentrations at the time of plating. Solvent treated (0.025% DMSO in medium) cells were used as control for etoposide. Medium treated cells were used as control for carboplatin and doxorubicin. To assess cell viability, treated cells were subjected to a quantification of nuclear fragmentation or ATP content. To measure the level of nuclear fragmentation, cell pellet (500,000 cells) was resuspended in 0.1% sodium citrate, pH 7.4, 0.05% Triton X-100, and 50 μg/ml propidium iodide. After resuspension, cells were incubated 2 to 4 hrs in the dark at 4°C. The percent of subG1 nuclei (fragmented DNA) was determined by flow cytometry. To measure the cellular ATP content, cells were reverse transfected with siRNAs in a 96 well plate at 1000 cells per well. 96 hours after transfection, media in each well was replaced with 70 µl of fresh media and 70 µl of CellTiter‐Glo cell viability reagent (Promega). The plates were shaken for 5 min and incubated at room temperature for 15 min. Luminescence was then read on the BioTek Cytation 5.

RNA-Seq analysis

For RNA-Seq data in **Fig. 5a**, 50,000 cells/well HeyA8 cells were reversed transfected in duplicate in 6-well plates with 10 nM of either pre-miR-34a-5p or si-miR-34a-5p^{Seed} with their respective controls. The transfection mix was replaced 24 hours after transfection. Cells were lysed 48 hours after transfection using Qiazol. For the RNA-Seq data in **Supplementary Figure 9**, HeyA8 cells were seeded at 50,000 cells per well in a 6-well plate and treated with three genotoxic drugs in duplicate: carboplatin (25 µg/ml), doxorubicin (50 ng/ml), and etoposide (500 nM). Medium treated cells were used as control for carboplatin and doxorubicin treated cells. Solvent control treated cells (0.025% DMSO in medium) were used as control for etoposide. Cells were lysed after 80 hours drug incubation using Qiazol. Total RNA was isolated using the miRNeasy Mini Kit (Qiagen, Cat.No# 74004) following the manufacturer's instructions. An on-column digestion step using the RNAse-free DNAse Set (Qiagen, Cat.No# 79254) was included for all RNA-Seq

samples. RNA libraries were generated and sequenced (Genomics Core facility at the University of Chicago). The quality and quantity of the RNA samples were checked using an Agilent bio-analyzer. Paired end RNA-SEQ libraries were generated using Illumina TruSEQ TotalRNA kits using the Illumina provided protocol (including a RiboZero rRNA removal step). Small RNA-SEQ libraries were generated using Illumina small RNA SEQ kits using the Illumina provided protocol. Two types of small RNA-SEQ sub-libraries were generated: one containing library fragments 140–150 bp in size and one containing library fragments 150–200 bp in size (both including the sequencing adaptor of about 130 bp). All three types of libraries (one RNA-SEQ and two small RNA-SEQ) were sequenced on an Illumina HiSEQ4000 using Illumina provided reagents and protocols. Adaptor sequences were removed from sequenced reads using TrimGalore (https://www.bioinformatics.babraham.ac.uk/projects/trim_galore), The trimmed reads were aligned to the hg38 version of the human genome, using either Tophat v2.1.0 (RNA-Seq data in **Supplementary Figure 9**) or STAR v2.5.2 (RNA-Seq data in **Fig. 5a**). In either case, aligned reads were associated with genes using HTSeq v0.6.1, and the UCSC hg38 transcriptome annotation from iGenomes. Differentially expressed genes were identified using the edgeR R package.

Arrayed real-time PCR

The top 30 most downregulated survival genes shared among HeyA8 cells treated with carboplatin, doxorubicin, and etoposide based on the RNA-Seq analysis were selected for a kinetics analysis using real-time PCR. To prepare the RNAs for the kinetics analysis, 75,000/plate HeyA8 cells were plated in 15 cm plates. Twenty-four hours after plating, one plate of HeyA8 cells were lysed in QIAzol as the control sample. The rest of the plates were treated with 50 ng/ml doxorubicin for 7 hrs, 14.5 hrs, and 21 hrs respectively before being lysed in QIAzol. To perform the arrayed real-time PCR, 200 ng total RNA per sample was used as the input to make cDNA using the high-capacity cDNA reverse Transcription Kit (Applied Biosystems #4368814). For TaqMan Low Density Array (TLDA) profiling, custom-designed 384-well TLDA cards (Applied Biosystems, Cat. No#4346799) were selected and used according to the manufacturer's protocols. For each sample, 20 µl cDNA was mixed with 80 µl water and 100 µl TaqMan Universal PCR Master Mix (Applied Biosystems, Cat. No#4304437). A total volume of 100µl of each sample is loaded into the 8 loading ports on the TLDA card (2 ports for each sample, 4 samples total on one card). The qPCR assays used to detect the 30 genes on the TLDA card are as follows: HIST1H2AI (Hs00361878_s1), CENPA (Hs00156455_m1), HJURP (Hs00251144_m1), FAM72D (Hs00416746_m1), CCNA2 (Hs00996788_m1), KIF20A (Hs00993573_m1), PRC1 (Hs01597839_m1), KIF15 (Hs01085295_m1), BUB1B (Hs01084828_m1), SCD (Hs01682761_m1), AURKA (Hs01582072_m1), NUF2 (Hs00230097_m1), NCAPH (Hs01010752_m1), SPC24 (Hs00699347_m1), KIF11 (Hs00189698_m1), TTK (Hs01009870_m1), PLK4 (Hs00179514_m1), AURKB (Hs00945858_g1), CEP55 (Hs01070181_m1), HMGCS1

(Hs00940429_m1), TOP2A (Hs01032137_m1), KIF23 (Hs00370852_m1), INCENP (Hs00934447_m1), CDK1 (Hs00938777_m1), HIST2H2BE (Hs00269023_s1), KNL1 (Hs00538241_m1), NCAPD2 (Hs00274505_m1), RACGAP1 (Hs01100049_mH), SPAG5 (Hs00197708_m1), KNTC1 (Hs00938554_m1). GAPDH (Hs99999905_m1) was used as the endogenous control. qPCR assay for individual gene was done in technical triplicates on each TLDA cards. Statistically analysis was performed using Student's t test.

Ago affinity peptide purification

To express and purify the FLAG-GST-T6B WT and mutant, constructs were expressed in BL21-Gold(DE3)pLysS competent cells (Agilent). Bacteria, induced with 1 mM Isopropyl β-D-1-thiogalactopyranoside (IPTG), were grown in 1 L overnight at 18ºC to OD 0.6. The bacteria were sedimented at 4000*g* for 15 min and resuspended in 25 ml GST-A buffer (1 mM 4-(2-aminoethyl) benzenesulfonyl fluoride hydrochloride (AEBSF), 1 mM DTT in PBS) supplemented with 1 mg/mL lysozyme (Sigma). Samples were sonicated three times for 3 min at 100% amplitude (Sonics, VCX130) and cleared by centrifugation at 20,000*g* for 20 min. The lysate was loaded onto a column containing 2 ml of bead volume glutathione Sepharose beads (Sigma) and washed two times with GST-A buffer. The GST-tagged protein was eluted in 10 ml of GST-B buffer (20 mM Tris, pH 8.0, and 10 mM glutathione in PBS). The peptide was concentrated using Amicon Ultra-15 Centrifugal Filter Unit (Millipore) and desalted using Zeba Spin Desalting Columns (ThermoFisher).

Ago pull down and small RNA-seq

HeyA8 (5-7 x 10^6), HCT116 wild-type (1.2-1.6 x 10^8) or *Drosha* k.o. (4.8-6.3 x 10^7) cells treated with doxorubicin were lysed in NP40 lysis buffer (20 mM Tris, pH 7.5, 150 mM NaCl, 2 mM EDTA, 1% (v/v) NP40, supplemented with phosphatase inhibitors) on ice for 15 minutes. The lysate was sonicated 3 times for 30 s at 60% amplitude (Sonics, VCX130) and cleared by centrifugation at 12,000*g* for 20 minutes. AGO1-4 were pulled down by using 500 µg of Flag-GST-T6B peptide [42] and with 60 µl anti-Flag M2 magnetic beads (Sigma-Aldrich) for 2 hrs at 4°C. The pull-down was washed 3 times in NP40 lysis buffer. During the last wash, 10% of beads were removed and incubated at 95°C for 5 minutes in 2x SDS-PAGE sample buffer. Samples were run on a 4-12% SDS-PAGE and transferred to nitrocellulose membrane. The pull-down efficiency was determined by immunoblotting against AGO2 (Abcam 32381). To the remaining beads 500 µl TRIzol reagent were added and the RNA extracted according to the manufacturer's instructions. The RNA pellet was diluted in 20 µl of water. The sample was split and half of the sample was dephosphorylated with 0.5 U/µl of CIP alkaline phosphatase at 37°C for 15 min and subsequently radiolabeled with 0.5 µCi γ-^{32}P-ATP and 1 U/µl of T4 PNK kinase for 20 min at 37°C. The AGO1-4 interacting RNAs were visualized on a 15% urea-PAGE. To prepare a small RNA library, RNA was ligated with 3' adenylated adapters and

separated on a 15% denaturing urea-PAGE. The RNA corresponding to insert size of 19-35 nt was eluted from the gel, ethanol precipitated followed by 5' adapter ligation. The samples were separated on a 12% Urea-PAGE and extracted from the gel. Reverse transcription was performed using Superscript III reverse transcriptase and the cDNA amplified by PCR. The cDNA was sequenced on Illumina HiSeq 3000.

Adapter sequences:

Adapter 1 – NNTGACTGTGGAATTCTCGGGTGCCAAGG;

Adapter 2 – NNACACTCTGGAATTCTCGGGTGCCAAGG,

Adapter 3 – NNACAGAGTGGAATTCTCGGGTGCCAAGG,

Adapter 4 – NNGCGATATGGAATTCTCGGGTGCCAAGG,

Adapter 47 – NNTCTGTGTGGAATTCTCGGGTGCCAAGG,

Adapter 48 – NNCAGCATTGGAATTCTCGGGTGCCAAGG,

Adapter 49 – NNATAGTATGGAATTCTCGGGTGCCAAGG,

Adapter 50 – NNTCATAGTGGAATTCTCGGGTGCCAAGG.

RT primer sequence: GCCTTGGCACCCGAGAATTCCA;

PCR primer sequences:

CAAGCAGAAGACGGCATACGAGATCGTGATGTGACTGGAGTTCCTTGGCACCCGAGAATTCCA.

Data analyses

GSEA was performed using the GSEA software version 3.0 from the Broad Institute downloaded from https://software.broadinstitute.org/gsea/. A ranked list was generated by sorting genes according the Log_{10}(fold downregulation). The Pre-ranked function was used to perform GSEA using the ranked list. 1000 permutations were used. Default settings were used. The ~1800 survival genes and ~420 non-survival genes defined previously [20] were used as custom gene sets. Default settings were used.

The list of survival genes and expression matched non-survival genes were generated by taking the survival and expression matched non-survival genes used previously (*20*) and retaining only the 938 genes in each group of expression matched survival and non-survival genes with an average expression across all RNA seq datasets above 1000 RPMs (see **Supplementary Data File 6**).

Sylamer analysis [29] was used to find enrichment of small word motifs in the 3'UTRs of genes enriched in those that are most downregulated. 3'UTRs were used from Ensembl, version 76. As required by Sylamer, they were cleaned of low-complexity sequences and repetitive fragments using respectively Dust [55] with default parameters and the RSAT interface [56] to the Vmatch program, also run with default parameters. Sylamer (version 12–342) was run with the Markov correction parameter set to 4. Bonferroni adjusted p-values were calculated by multiplying the unadjusted p-values by the number of permutations for each length of word searched for.

The GO enrichment analyses shown in **Fig. 5b** and **Supplementary Figure 6b** were performed using the GOrilla GO analysis tool at http://cbl-gorilla.cs.technion.ac.il using default setting using different p-value cut-offs for each analysis. GO analysis in **Supplementary Data File 5** was done using DAVID 6.8 (https://david.ncifcrf.gov) using default settings. GO analyses across multiple data sets were performed using the software available on www.Metascape.org and default running parameters.

Density plots showing the contribution of the four nucleotides G, C, A and U at each of the 6mer seed positions were generated using the Weblogo tool at http://weblogo.berkeley.edu/logo.cgi using the frequency plot setting.

Venn diagrams were generated using http://bioinformatics.psb.ugent.be/webtools/Venn/ using default settings.

The scatter plot in **Fig. 5a** was generated using R package ggplot2. 10875 genes with RPM > 1 (average RPM of the 8 RNAseq samples) and adjusted p-value < 0.05 were included. 3696 genes were significantly upregulated in both mir-34a-5p and si34a-5p^{Seed} treated samples. 4207 genes were significantly downregulated in both mir-34a-5p and si34a-5p^{Seed} treated samples. 713 genes were only downregulated and 792 genes were only upregulated in si34a-5p^{Seed} treated samples. 730 genes were only downregulated and 737 genes were only upregulated in mir-34a-5p treated samples. 193 genes out of the total 10875 genes were omitted in the graph as the range for X and Y axes were set as -3 to 3.

Identification of the most and least toxic 6mer seeds

To identify the 20 and 100 most and least toxic seeds to both human cell lines all 4096 seeds were ranked for each cell line from highest to lowest toxicity. The 20 seeds with the highest toxicity to both HeyA8 and H460 cells were found in the top 46 most toxic seeds to in both cells and the 20 seeds shared to be least toxic were found in the bottom 149 seeds in each ranked group. The 100 most and least toxic seeds for both cell lines were identified in the same way and all groups of seeds are shown in **Supplementary Data File 2**.

Metaplots of 6-mer seed match locations

3'UTR sequences were downloaded from Ensembl Biomart. In order to reduce redundancy in the sequences, a single longest 3'UTR (and associated transcript) was chosen to represent each gene. A custom perl script (makeSeedBed.pl) was written to identify exact matches to all seeds (reverse complement) in all sequences, and to output the coordinates of those matches in bed file format. A custom R script (plotBedMetaPlot.R) was written that uses the GenomicRanges [57] and Sushi [58] R packages to calculate the coverage of seeds across all sequences in a given set, and to create a plot of that coverage. The custom scripts and the input data are available in the cloud-based computational reproducibility platform Code Ocean at https://codeocean.com/capsule/31ec8deb-8282-4a90-98e6-b80a0ba881cb/code.

eCDF plots

A custom perl script (annotateWithSeeds.pl) was written to identify exact seed matches (reverse complement) to all seeds in all sequences, and to output the total counts of the different types of seeds (generally toxic vs. nontoxic) in the sequences. To compare the presence of toxic and nontoxic seed matches in expression matched survival and non survival genes, a custom R script (makeECDFplot.180615.R) was written that takes as input two different sets of genes (SGs and nonSGs) and the list of the counts of toxic and nontoxic seeds (reverse complement) in all genes, and plots the cumulative distribution function for the count statistics in each gene set. In **Fig. 3b** the ratio of the seed match counts to the 20 most and least toxic seeds in the 5'UTR, CDS, first 1000bp of 3'UTR, and full 3'UTR (not shown) were compared between pairs of 938 expression matched survival and non-survival genes. In **Supplementary Figure 5a**, this analysis was repeated with the 100 most and least toxic seeds to both human cell lines. The custom scripts and the input data are available in the cloud-based computational reproducibility platform Code Ocean at https://codeocean.com/capsule/b755ec2b-00d8-4281-9fa1-2a484fd7521b/code. To determine the dependence of mRNAs regulation on miR-34a-5p seed presence in their 3'UTR, a custom R script (makeECDFplot.cetoData.R) was written that takes as input a list of gene sets and a table of logFC expression for those genes upon miR-34a-5p or si34a-5p^{Seed} over-expression. This Rscript then plots the cumulative distribution function for the logFC expression data in each gene set. The custom scripts and the input data are available in the Code Ocean at https://codeocean.com/capsule/31ec8deb-8282-4a90-98e6-b80a0ba881cb/code.

Relation between miRNA seed conservation, age and toxicity

Information on miRNA seed family conservation and seed sequence were downloaded at http://www.targetscan.org/vert_71/ from TargetScan Human 7.1. The toxicity of each mature human miRNA arm sequence in the TargetScan dataset was assigned according to the average toxicity induced by the siRNA in HeyA8 and H460 siRNA screens harboring the identical 6mer seed sequence. A list of miRNA ages corresponding to ~1025 miRNA loci was acquired from [31] and was calculated using a modified version of ProteinHistorian [31]. This list was used to assign ages to roughly ~1400 mature miRNA arms found in the TargetScan dataset.

TargetScan 7.1 partitions the seed family conservation into four groups: highly conserved (group #2), conserved (group #1), low conservation but still annotated as a miRNA (group #0), and low conservation with the possibility of misannotation (group #-1). Probability density and eCDF plots for the assigned 6mer seed-dependent toxicities were generated for each seed family conservation group as defined by Targetscan (groups -1, 0, 1, and 2) using ggplot2 in R. Probability density and eCDF plots were also generated to show

how young (<10 million years) and old (>800 million years) miRNAs compare in terms of the seed-dependent toxicity. All differences between groups in terms of seed-dependent toxicity (always the average of the toxicity determined in HeyA8 and H460 cells) were analyzed using a two-sample two-tailed Kolmogorov-Smirnov test in R.

Assessment of dominant arm seed toxicity

The expression (RPM) of miRNA 5p and 3p arms across 135 tissue samples were collected from MIRMINE [59]. A miRNA was considered expressed if the sum of the normalized reads for both arms was above 5 for each sample. A value of 0 was replaced with 0.01 to avoid a division by 0 error. A miRNA arm was considered the dominant species if its expression was at least 25% greater than the other arm per sample. The dominant arm for each miRNA across all samples was calculated by determining which arm was dominantly expressed in more samples (>50% of samples where the miRNA was considered expressed). The miRNAs that have only one annotated arm in miRBase were considered to have only one dominant arm. The seed toxicity values for each arm were extracted from the 4096 siRNA screen data (% average viability for the human HeyA8 and H460 cells) and used to calculate the ratio between the dominant arm's toxicity and the lesser arm's toxicity; miRNAs that only had one expressed arm were not considered in the analyses shown in **Fig. 6d** but are all included on the website: 6merdb.org.

To compare the 6mer seed toxicity between up regulated and down regulated Ago bound miRNA populations in HCT116 cells after Doxo treatment we analyzed the reads obtained from RNA Seq analysis of Ago bound RNAs. After removing the reads that were either shorter than 19 nt or longer than 26 nt in length, the reads were blasted against a miRNA database consisting of all human miRNA mature sequence information obtained from miRBase. A threshold of 100% identity for an at least 16 nt-long stretch without any gaps was set for the BLAST analysis. After discarding sequences with no significant BLAST result, the remaining sequences were trimmed from the 3'end so that all reads were now 19nt in length. This was done to determine for each miRNA the relevant 5' end to obtain the 6mer seed sequence (position 2-7). All the reads that shared the same 5' sequence and miRNA names were collapsed while adding up the number of reads of each sequence in each condition. To compare the 6mer seed toxicity between up and down regulated miRNAs, we calculated the average 6mer seed toxicity for miRNA sequences that were either 1.5 fold up or 1.5 fold down regulated in Doxo treated wt samples compared to medium treated control samples (after removing sequences that had less than 100 collapsed reads in Doxo treated wt samples). In each group miRNAs were ranked according to highest base mean expression and groups were compared (**Fig. 7d**). Statistically significance was determined using the Wilcoxon rank test. The comparison was repeated for *Drosha* k.o. cells where the 5' shifted form of miR-320a-3p was the only miRNA found to be upregulated (1.5 fold).

Analysis of miRtron and non-miRtron groups

MiRtrons and non-miRtrons were recently reported [60] and consisted of miRNAs that are listed in miRBase v21 as expressing both arms. Comparing 6mer toxicity of miRtrons and non-miRtrons from this list was done as described above for young/old non-conserved/conserved miRNAs. Both arms were considered. Probability density (**Fig. 6c**) and eCDF plots (**Supplementary Figure 7c**) were generated to show how miRtrons and non-miRtrons compare in terms of the seed-dependent toxicity. To calculate the 6mer toxicity across the entire miRtron sequences, we extracted all possible 6-nt stretches from the first 17nts of the 428 mature miRtron sequences beginning at the 5'end using a 6nt sliding window (12 different start positions in total). The first 17nts were chosen because all miRtrons sequences are 17-25nt in length. Average 6mer toxicity of the 428 miRtrons was calculated for each start position and plotted in **Supplementary Figure 7e**. To visualize the nucleotide content across of all miRtrons, the first 8 nucleotides from the 5'end or the last 8 nucleotides from the 3'end were extracted from the 428 mature miRtron sequences and analyzed using the Weblogo tool.

Seed viability of shRNAs derived from the CD95L sequence

An RNAi lethality screen composed of every shRNA sequence that can be derived from the CD95L CDS was conducted previously (*20*). In this screen, toxicity of each shRNA was assessed in two ways: 1) fold underrepresentation of the shRNA after infection with the shRNA-expressing lentivirus compared to its representation in the plasmid pool and 2) fold representation of the shRNA after infection and treatment with doxycycline compared to cells that were infected but did not receive doxycycline. The first analysis allowed us to quantify toxicity associated with leaky shRNA expression. The second analysis quantified toxicity associated with strong shRNA expression following treatment with doxycycline.

For each shRNA, the average fold downregulation was calculated from both of these toxicity assessments. Then, the seed sequence of each shRNA was extracted and assigned an average viability score, which was a composite of the % viabilities determined in the 4096 siRNA arrayed screen for both HeyA8 and H460 cells.

Pearson's correlation was determined for each CD95L-derived shRNA between its associated fold downregulation in the screen (*20*) and the average seed sequence viability determined in the 4096 siRNA screen.

In addition, the CD95L shRNAs were split into two groups: 1) 137 shRNAs with an average fold downregulation (as determined in the shRNA lethality screen) above 5 and 2) a control group with a matching number of shRNAs whose fold deregulation had an absolute value closest to 0. The average seed viability (as determined from the siRNA screen) was extracted for the shRNAs in these two groups and compared using the two-sample, two-tailed Rank Sum test.

Statistical analyses

Continuous data were summarized as means and standard deviations (except for all IncuCyte experiments where standard errors are shown) and dichotomous data as proportions. Continuous data were compared using t-tests for two independent groups and one-way ANOVA for 3 or more groups. For evaluation of continuous outcomes over time, two-way ANOVA was performed using the Stata 14 software with one factor for the treatment conditions of primary interest and a second factor for time treated as a categorical variable to allow for non-linearity. Comparisons of single proportions to hypothesized null values were evaluated using binomial tests. Statistical tests of two independent proportions were used to compare dichotomous observations across groups. Pearson correlation coefficients (r) and p - values as well as Wilcoxon rank test were calculated using StatPlus (v. 6.3.0.5). Kolmogorov–Smirnov two-sample two-sided test was used to compare different probability distributions shown in all density plots and eCDF plots. Wilcoxon rank sum test was used to test for statistical significance in the analysis of the toxicity all miRNA arms in **Fig. 6d**. The Fisher Exact Test was used to calculate p-values in **Fig. 6b** to determine whether the percent frequency of G versus non-G (A, C, and U) nucleotides at each position along the 6mer seed was different between young (<10M years) and ancient (>800M years) miRNAs. The effects of treatment vs. control over time were compared for *Drosha* k.o. and wild-type cells by fitting regression models that included linear and quadratic terms for value over time, main effects for treatment and cell type, and two- and three-way interactions for treatment, cell-type and time. The three-way interaction on the polynomial terms with treatment and cell type was evaluated for statistical significance since this represents the difference in treatment effects over the course of the experiment for the varying cell types.

Data availability

RNA sequencing data generated for this study is available in the GEO repository: GSE111379 (https://www.ncbi.nlm.nih.gov/geo/query/acc.cgi?acc=GSE111379, reviewer access token: srileyyktjctduz) and GSE111363 (https://www.ncbi.nlm.nih.gov/geo/query/acc.cgi?acc=GSE111363, reviewer access token: udedukauvjexbmp). All 6mer seed toxicity data of the 4096 siRNA screen in HeyA8, H460, M565, and 3LL cells are available in searchable form at https://6merdb.org. All source data are available upon request.

ACKNOWLEDGEMENTS

We are indebted to Dr. Leon Platanias for his generous support of the seed screen and to Denise Scholtens for help with biostatistics. M.H. was supported by the Intramural Research Program of NIAMS and A.A.S. by the Swedish Research Council postdoctoral fellowship. This work was funded by training grant T32CA009560 (to W.P.), R35CA197450 (to M.E.P.), R50CA221848 (to E.T.B.), and RO1 211916 (to EL).

AUTHOR CONTRIBUTIONS

M.E.P., Q.Q.G., W.E.P. and A.E.M. conceived the study. Q.Q.G., W.E.P. performed the majority of the experiments and data analysis. S.C. performed the 6mer seed screens. A.A.S. performed the Ago pull-down experiments. E.T.B. performed data analyses. J.M.P designed and implemented the website. M.H. provided critical conceptual input. M.E.P. designed the study, guided the interpretation of the results and drafted the manuscript. All authors discussed the results, edited and approved the draft and final versions of the manuscript.

DECLARATION OF INTEREST

The authors declare no competing interests.

Figure legends

Fig. 1 A comprehensive screen identifies the most toxic 6mer seeds. **a** Schematic of the siRNA backbone used in the 4096 seed duplexes toxicity screen. Red X: 2'-O-methylation modification; blue letters: constant nucleotides; red letters: variable 6mer seed sequence. **b** *Top:* Results of the 4096 6mer seed duplex screen in two human (top) and two mouse (bottom) cell lines. Cells were reverse transfected in triplicates in 384 well plates with 10 nM of individual siRNAs. The cell viability of each 6mer seed duplex was determined by quantifying cellular ATP content 96 hours after transfection. All 4096 6mer seeds are ranked by the average effect on cell viability of the four cell lines from the most toxic (left) to the least toxic (right). Rankings of the 6mer seeds of four previously characterized CD95L derived siRNAs (siL1, siL2, siL3, and siL4) are highlighted in green. We consider an siRNA highly toxic if it reduces cell viability 90% or more and moderately toxic if it reduces cell viability 50% or more (black stippled line). **c** Regression analysis showing correlation between the 6mer seed toxicity observed in the human lung cancer cell line H460 (y axis) and the matching 6mer toxicity observed in the human ovarian cancer cell line HeyA8 (x axis) (left) and average toxicity in the two human cell lines (y axis) and two mouse cell lines (x axis) (right). p-values were calculated using Pearson correlation analysis. **d** *Left:* Correlation between the $\log_{10}$ (fold down underrepresentation) of all possible shRNAs that can be derived from the mRNA sequence of CD95L following their expression from a DOX-inducible lentiviral vector [20] and the toxicity of their seed sequences as determined in a 4096 arrayed siRNA screen (average of both human cell lines). *Right*: Difference in average seed toxicity between the 137 CD95L-derived shRNAs downregulated at least 5 fold (= toxic) in this screen compared to a size matched group of 137 shRNAs that were the least altered in abundance in that screen. Pearson correlation coefficient is given as well as p-value (left) and p-value in analysis on the right was calculated using unpaired two-sided ttest. The center crossbar of the box plot represents the mean, and the upper/lower boundaries demark +/- 1 standard deviation.

Fig. 2 The most toxic seeds are G rich. **a** Cell viability of the 19 seed duplexes with the highest content (>80%) in the 6mer seed region for each nucleotide in two human and two mouse cell lines. Samples were analyzed in triplicate and mean ± SD for each sample is shown. p-values between groups of duplexes were calculated using Student's t-test. **b** Nucleotide composition at each of the 6 seed positions in the top 200 most toxic (left) or the top 200 least toxic (right) seed duplexes in the four cell lines. siRNAs are considered to be toxic when viability is inhibited >50% (grey stippled line).

Fig. 3 Toxic G-rich seed-containing duplexes target housekeeping genes enriched in Cs. **a** Nucleotide composition of 20 seeds that are most and least toxic in both human cell lines (see **Fig. 1b**). **b** eCDF

comparing the ratio of occurrences of the 20 most and least toxic 6mer seed matches in the mRNA elements of two sets of expression matched survival genes and nonsurvival genes. Significance was calculated using a two-sample two-sided Kolmogorov–Smirnov (K-S) test. **c** Probability density plots comparing the nucleotide content between the groups of expression matched SGs and nonSGs. p-values were calculated using a two-sample two-sided K-S test comparing the density distribution of SGs and nonSGs. Relevant peak maxima are given. **d** Single nucleotide frequency distribution in human mRNAs around the boundaries of the 5'UTR and the beginning of the CDS and the end of the CDS and the beginning of the 3'UTR (shown are 500 bases in each direction). Data are shown for either all human coding genes (top), or a set of 938 SGs or an expression matched set of 938 nonSGs (bottom four panels). Blue horizontal bars, area of reduced A/U content in SGs. p-values were calculated using a two-sample two-sided K-S test. **e** Distribution of the seed matches to the 20 most and least toxic 6mer seeds to human cells in human mRNAs around the boundaries of the 5'UTR and the beginning of the CDS and the end of the CDS and the beginning of the 3'UTR (shown are 500 bases in each direction). Data are shown for either all genes (top) or the expression matched SGs and nonSGs (center and bottom). Green horizontal bar, area of enriched toxic seed matches in SGs compared to nonSGs. Blue horizontal bar, area of fewer toxic seed matches in SGs.

Fig. 4 Tumor suppressive miRNAs inhibit cancer cell growth via toxic 6mer seeds. **a** All 4096 6mer seeds ranked from the lowest average viability (highest toxicity) to the highest viability (lowest toxicity) in HeyA8 and H460 cells. Locations of 6mer seeds present in major tumor suppressive (red) or tumor promoting (blue) miRNAs are highlighted as individual bars. miRNAs are considered to be toxic when viability is inhibited >50% (blue stippled line). **b** Percent cell confluence over time of HeyA8 cells transfected with 5 nM of either the indicated tumor suppressive miRNA precursors or a miRNA precursor nontargeting control. Data are representative of two independent experiments. Each data point represents mean ± SE of four replicates. *Two-way ANOVA p-value between cells treated with pre-miR-(NC) and pre-let-7a-5p is 0.0000. **c** *Left*: Percent cell confluence over time of HeyA8 parental cells transfected with either pre-miR-34a-5p or si34a-5p^{Seed} and compared to their respective controls (pre-miR (NC) for pre-miR-34a-5p and siNT2 for si34a-5p^{Seed}) at 10 nM. Data are representative of two independent experiments. Each data point represents mean ± SE of four replicates. *Right*: % cell death of the same cells harvested 4 days after transfection. Data are representative of two experiments. Each data point represents mean ± SD of three replicates. **d** Morphology of HeyA8 cells transfected with 10 nM of either pre-miR-34a-5p or si34a-5p^{Seed} compared to their respective controls three days after transfection.

Fig. 5 miR-34a-5p kills cancer cells through its toxic 6mer seed. **a** *Top*: Alignment of the sequences of miR-34a-5p and miR-34a-5p^{Seed} with the 6mer highlighted. *Bottom:* Comparison of deregulated mRNAs

(adjusted $p<0.05$, RPM > 1) in HeyA8 cells 48 hrs after transfection with either miR-34a-5p or si34a-5p^{Seed}. Pearson correlation p-value is given. **b** Overlap of RNAs detected by RNA-Seq downregulated in HeyA8 cells (>1.5 fold) 48 hrs after transfection with either si34a-5p^{Seed} or miR-34a-5p when compared to either siNT2 or a nontargeting pre-miR, respectively. *Right*: Results of a GOrilla gene ontology analyses of the genes downregulated in both cells transfected with miR-34a-5p or si34a-5p^{Seed} (top, significance of enrichment $<10^{-11}$), or only in cells transfected with miR-34a-5p (bottom, significance of enrichment $<10^{-4}$). **c** Sylamer plots for the list of 3'UTRs of mRNAs in cells treated with either miR-34a-5p (top) or si34-5p^{Seed} (bottom) sorted from down-regulated to up-regulated. The most highly enriched sequence is shown which, in each case, is the 6mer seed match of the introduced 6mer seed. Bonferroni-adjusted p-values are shown. **d** Gene set enrichment analysis for a group of 1846 survival genes (top 4 panels) and 416 non-survival genes (bottom 2 panels) [20] after transfecting HeyA8 cells with either miR-34a-5p or si34a-5p^{Seed}. siNT1 and a nontargeting premiR served as controls, respectively. p-values indicate the significance of enrichment.

Fig. 6 Toxic 6mer seeds and the evolution of cancer regulating miRNAs. **a** Probability density plot of cell viability of the 6mer seeds of either highly conserved (from humans to zebrafish) or poorly conserved miRNA seed families (left panel, total number of mature miRNAs = 2164) or of very old (>800 Million years) miRNAs or very young (<10 Million years) miRNAs (right panel, total number of miRNAs = 299). For the analysis on the right, miRNA arms with identical sequences (gene duplications) were collapsed and counted as one arm. Two-sample two-sided K-S test was used to calculate p-values. **b** Change in nucleotide composition in the 6mer seeds of miRNAs of different ages. Significance of change in nucleotide composition at each of the 6 seed positions between the youngest and oldest miRNAs was calculated using a Fisher's exact test. Note: the oldest miRNAs also contain tumor suppressive miRNAs with high G content in positions 1 and 2 which may be the reason the analysis in these two positions did not reach statistical significance. **c** Probability density plot of cell viability of the 6mer seeds of mature miRtrons or non-miRtrons. miRNAs with identical sequences (gene duplications) were collapsed and counted as one seed. Two-sample two-sided K-S test was used to calculate p-value. **d** 780 miRNAs (**Supplementary Data File 4**) ranked according to the ratio of viability of the seed (as determined in the seed screen) of the guide strand and the lesser-expressed arm. Established oncogenic miRNAs are shown in blue, tumor-suppressive miRNAs are shown in red. The guide strand is given for each miRNA (in parenthesis). p-value of the distribution of oncogenic versus tumor suppressive miRNAs was calculated using Wilcoxon rank test. **e** Cumulative read numbers from the 5p or the 3p arm (according to miRBase.org) of three oncogenic and three tumor-suppressive miRNAs with the highest (top three) or lowest (bottom three) ratio of the viability of the guide strand versus the lesser arm. The viability numbers of the matching 6mer seeds according to the

siRNA 6mer seed screen are given. The sequences of the mature 5p or 3p arms are boxed in blue and black, respectively. Toxic seeds are shown in red, non-toxic ones in blue.

Fig. 7 Genotoxic drugs cause upregulation of tumor suppressive miRNAs with toxic 6mer seeds. **a** *Top*: Autoradiograph of radiolabeled RNAs pulled down with the Ago proteins from HeyA8 cells treated with doxorubicin (Doxo) for different times. *Bottom*: Western blot for the pulled down AGO2 of the same samples shown above. The images are representative of two biological duplicates. **b** Fold change of the total reads of Ago bound small RNAs after 20, 40, or 80 hours of Doxo treatment compared to the control sample from Ago-IP sequencing data (Ago bound). Fold change of the total reads of cytosolic small RNAs in HeyA8 cells treated with Doxo for 80 hours compared to the control sample from small RNA-Seq data is given (Total). Data are the combination of biological duplicates. **c** Pie charts showing the composition of miRNAs bound to Ago proteins after 50 hrs Doxo treatment in HCT116 wild-type (left) or *Drosha* k.o. cells (right). **d** *Left*, 6mer seed viability (average between HeyA8 and H460 cells, two replicates) of the Ago-bound miRNAs most up and downregulated in wt or *Drosha* k.o. cells after Doxo treatment. K-S test was used to calculate p-value. *Right*, Comparison of the predicted (and most abundant) sequence of miR-320a-3p and Ago-bound sequence of miR-320a-3p and their average viability found most upregulated in *Drosha* k.o. cells after Doxo treatment. Shown is variance of two biological replicates. **e** Percent cell confluence over time of HeyA8 cells transfected with 5 nM of controls, pre-miR-320a-3p or an siRNA duplex that corresponds to the shifted form of miR-320a-3p (si-miR-320a-3p^{Ago}) that was found to be upregulated and bound to Ago proteins upon Doxo treatment. Data are representative of two independent experiments. Each data point represents mean ± SE of four replicates. **f** Viability changes (ATP content) in four cell lines 96 hrs after transfection with Lipid only, 10 nM of siNT1, siL3, a nontargeting pre-miR, or miR-320a-3p^{Ago} - the only shared upregulated miRNA in HeyA8 cells, HCT116 wild-type, and HCT116 *Drosha* k.o. cells - after Doxo treatment. p-values were determined using Student's t-test. *** $p<0.0001$. Samples were performed in triplicate (siNT1, siL3), 6 repeats (miR-320a-3p^{Ago}) and 8 repeats (Lipid).

REFERENCES

1. Lee Y, *et al.* MicroRNA genes are transcribed by RNA polymerase II. *EMBO J* **23**, 4051-4060 (2004).

2. Han J, Lee Y, Yeom KH, Kim YK, Jin H, Kim VN. The Drosha-DGCR8 complex in primary microRNA processing. *Genes Dev* **18**, 3016-3027 (2004).

3. Yi R, Qin Y, Macara IG, Cullen BR. Exportin-5 mediates the nuclear export of pre-microRNAs and short hairpin RNAs. *Genes Dev* **17**, 3011-3016 (2003).

4. Bernstein E, Caudy AA, Hammond SM, Hannon GJ. Role for a bidentate ribonuclease in the initiation step of RNA interference. *Nature* **409**, 363-366 (2001).

5. Hutvagner G, McLachlan J, Pasquinelli AE, Balint E, Tuschl T, Zamore PD. A cellular function for the RNA-interference enzyme Dicer in the maturation of the let-7 small temporal RNA. *Science* **293**, 834-838 (2001).

6. Wang Y, Sheng G, Juranek S, Tuschl T, Patel DJ. Structure of the guide-strand-containing argonaute silencing complex. *Nature* **456**, 209-213 (2008).

7. Leuschner PJ, Ameres SL, Kueng S, Martinez J. Cleavage of the siRNA passenger strand during RISC assembly in human cells. *EMBO Rep* **7**, 314-320 (2006).

8. Schirle NT, MacRae IJ. The crystal structure of human Argonaute2. *Science* **336**, 1037-1040 (2012).

9. Eulalio A, Huntzinger E, Izaurralde E. GW182 interaction with Argonaute is essential for miRNA-mediated translational repression and mRNA decay. *Nat Struct Mol Biol* **15**, 346-353 (2008).

10. Lewis BP, Shih IH, Jones-Rhoades MW, Bartel DP, Burge CB. Prediction of mammalian microRNA targets. *Cell* **115**, 787-798 (2003).

11. Lai EC. Micro RNAs are complementary to 3' UTR sequence motifs that mediate negative post-transcriptional regulation. *Nat Genet* **30**, 363-364 (2002).

12. Selbach M, Schwanhausser B, Thierfelder N, Fang Z, Khanin R, Rajewsky N. Widespread changes in protein synthesis induced by microRNAs. *Nature* **455**, 58-63 (2008).

13. Baek D, Villen J, Shin C, Camargo FD, Gygi SP, Bartel DP. The impact of microRNAs on protein output. *Nature* **455**, 64-71 (2008).

14. Esquela-Kerscher A, Slack FJ. Oncomirs - microRNAs with a role in cancer. *Nat Rev Cancer* **6**, 259-269 (2006).

15. Balatti V, Pekarky Y, Rizzotto L, Croce CM. miR deregulation in CLL. *Adv Exp Med Biol* **792**, 309-325 (2013).

16. Slabakova E, Culig Z, Remsik J, Soucek K. Alternative mechanisms of miR-34a regulation in cancer. *Cell Death Dis* **8**, e3100 (2017).

17. Hua YJ, Larsen N, Kalyana-Sundaram S, Kjems J, Chinnaiyan AM, Peter ME. miRConnect 2.0: Identification of antagonistic, oncogenic miRNA families in three human cancers. *BMC Genomics* **14**, 179 (2013).

18. Concepcion CP, Bonetti C, Ventura A. The microRNA-17-92 family of microRNA clusters in development and disease. *Cancer journal* **18**, 262-267 (2012).

19. He X, He L, Hannon GJ. The guardian's little helper: microRNAs in the p53 tumor suppressor network. *Cancer Res* **67**, 11099-11101 (2007).

20. Putzbach W, *et al.* Many si/shRNAs can kill cancer cells by targeting multiple survival genes through an off-target mechanism. *eLife* **6**, e29702 (2017).

21. Murmann AE, *et al.* Induction of DISE in ovarian cancer cells in vivo. *Oncotarget* **8**, 84643-84658 (2017).

22. Murmann AE, *et al.* Small interfering RNAs based on huntingtin trinucleotide repeats are highly toxic to cancer cells. *EMBO Rep* **19**, e45336 (2018).

23. Putzbach W, *et al.* CD95/Fas ligand mRNA is toxic to cells. In revision. Preprint at BiorXiv. https://doi.org/10.1101/330324 (2018).

24. Hadji A, *et al.* Death induced by CD95 or CD95 ligand elimination. *Cell Reports* **10**, 208-222 (2014).

25. Bramsen JB, *et al.* A large-scale chemical modification screen identifies design rules to generate siRNAs with high activity, high stability and low toxicity. *Nucleic Acids Res* **37**, 2867-2881 (2009).

26. Peter ME. Let-7 and miR-200 microRNAs: guardians against pluripotency and cancer progression. *Cell Cycle* **8**, 843-852 (2009).

27. Agostini M, Knight RA. miR-34: from bench to bedside. *Oncotarget* **5**, 872-881 (2014).

28. Patel M, Peter ME. Identification of DISE-inducing shRNAs by monitoring cellular responses. *Cell Cycle* **17**, 506-514 (2018).

29. van Dongen S, Abreu-Goodger C, Enright AJ. Detecting microRNA binding and siRNA off-target effects from expression data. *Nat Methods* **5**, 1023-1025 (2008).

30. Grimson A, Farh KK, Johnston WK, Garrett-Engele P, Lim LP, Bartel DP. MicroRNA targeting specificity in mammals: determinants beyond seed pairing. *Mol Cell* **27**, 91-105 (2007).

31. Patel VD, Capra JA. Ancient human miRNAs are more likely to have broad functions and disease associations than young miRNAs. *BMC Genomics* **18**, 672 (2017).

32. Berezikov E, Chung WJ, Willis J, Cuppen E, Lai EC. Mammalian mirtron genes. *Mol Cell* **28**, 328-336 (2007).

33. Meijer HA, Smith EM, Bushell M. Regulation of miRNA strand selection: follow the leader? *Biochem Soc Trans* **42**, 1135-1140 (2014).

34. Concepcion CP, *et al.* Intact p53-dependent responses in miR-34-deficient mice. *PLoS Genet* **8**, e1002797 (2012).

35. Meredith AM, Dass CR. Increasing role of the cancer chemotherapeutic doxorubicin in cellular metabolism. *J Pharm Pharmacol* **68**, 729-741 (2016).

36. Yeung TK, Germond C, Chen X, Wang Z. The mode of action of taxol: apoptosis at low concentration and necrosis at high concentration. *Biochem Biophys Res Commun* **263**, 398-404 (1999).

37. Yoo SH, *et al.* Etoposide induces a mixed type of programmed cell death and overcomes the resistance conferred by Bcl-2 in Hep3B hepatoma cells. *Int J Oncol* **41**, 1443-1454 (2012).

38. Kwon HK, *et al.* Etoposide Induces Necrosis Through p53-Mediated Antiapoptosis in Human Kidney Proximal Tubule Cells. *Toxicol Sci* **148**, 204-219 (2015).

39. Wang D, Lippard SJ. Cellular processing of platinum anticancer drugs. *Nat Rev Drug Discov* **4**, 307-320 (2005).

40. Chang BD, *et al.* A senescence-like phenotype distinguishes tumor cells that undergo terminal proliferation arrest after exposure to anticancer agents. *Cancer Res* **59**, 3761-3767 (1999).

41. Eom YW, *et al.* Two distinct modes of cell death induced by doxorubicin: apoptosis and cell death through mitotic catastrophe accompanied by senescence-like phenotype. *Oncogene* **24**, 4765-4777 (2005).

42. Hauptmann J, *et al.* Biochemical isolation of Argonaute protein complexes by Ago-APP. *Proc Natl Acad Sci U S A* **112**, 11841-11845 (2015).

43. Kim YK, Kim B, Kim VN. Re-evaluation of the roles of DROSHA, Export in 5, and DICER in microRNA biogenesis. *Proc Natl Acad Sci U S A* **113**, E1881-1889 (2016).

44. Walz AL, *et al.* Recurrent DGCR8, DROSHA, and SIX homeodomain mutations in favorable histology Wilms tumors. *Cancer Cell* **27**, 286-297 (2015).

45. Kumar MS, Lu J, Mercer KL, Golub TR, Jacks T. Impaired microRNA processing enhances cellular transformation and tumorigenesis. *Nat Genet* **39**, 673-677 (2007).

46. Chandradoss SD, Schirle NT, Szczepaniak M, MacRae IJ, Joo C. A Dynamic Search Process Underlies MicroRNA Targeting. *Cell* **162**, 96-107 (2015).

47. Di Martino MT, *et al.* Synthetic miR-34a mimics as a novel therapeutic agent for multiple myeloma: in vitro and in vivo evidence. *Clin Cancer Res* **18**, 6260-6270 (2012).

48. Beg MS, *et al.* Phase I study of MRX34, a liposomal miR-34a mimic, administered twice weekly in patients with advanced solid tumors. *Invest New Drugs* **35**, 180-188 (2017).

49. Cao W, *et al.* miR-34a regulates cisplatin-induce gastric cancer cell death by modulating PI3K/AKT/survivin pathway. *Tumour Biol* **35**, 1287-1295 (2014).

50. Navarro F, Lieberman J. miR-34 and p53: New Insights into a Complex Functional Relationship. *PLoS One* **10**, e0132767 (2015).

51. Alfano L, Costa C, Caporaso A, Antonini D, Giordano A, Pentimalli F. HUR protects NONO from degradation by mir320, which is induced by p53 upon UV irradiation. *Oncotarget* **7**, 78127-78139 (2016).

52. Stark A, Brennecke J, Bushati N, Russell RB, Cohen SM. Animal MicroRNAs confer robustness to gene expression and have a significant impact on 3'UTR evolution. *Cell* **123**, 1133-1146 (2005).

53. Zare H, Khodursky A, Sartorelli V. An evolutionarily biased distribution of miRNA sites toward regulatory genes with high promoter-driven intrinsic transcriptional noise. *BMC Evol Biol* **14**, 74 (2014).

54. Ceppi P*, et al.* CD95 and CD95L promote and protect cancer stem cells. *Nature Commun* **5**, 5238 (2014).

55. Morgulis A, Gertz EM, Schaffer AA, Agarwala R. A fast and symmetric DUST implementation to mask low-complexity DNA sequences. *J Comput Biol* **13**, 1028-1040 (2006).

56. Medina-Rivera A*, et al.* RSAT 2015: Regulatory Sequence Analysis Tools. *Nucleic Acids Res* **43**, W50-56 (2015).

57. Lawrence M*, et al.* Software for computing and annotating genomic ranges. *PLoS Comput Biol* **9**, e1003118 (2013).

58. Phanstiel DH, Boyle AP, Araya CL, Snyder MP. Sushi.R: flexible, quantitative and integrative genomic visualizations for publication-quality multi-panel figures. *Bioinformatics* **30**, 2808-2810 (2014).

59. Panwar B, Omenn GS, Guan Y. miRmine: a database of human miRNA expression profiles. *Bioinformatics* **33**, 1554-1560 (2017).

60. Rorbach G, Unold O, Konopka BM. Distinguishing mirtrons from canonical miRNAs with data exploration and machine learning methods. *Sci Rep* **8**, 7560 (2018).

Figure 1

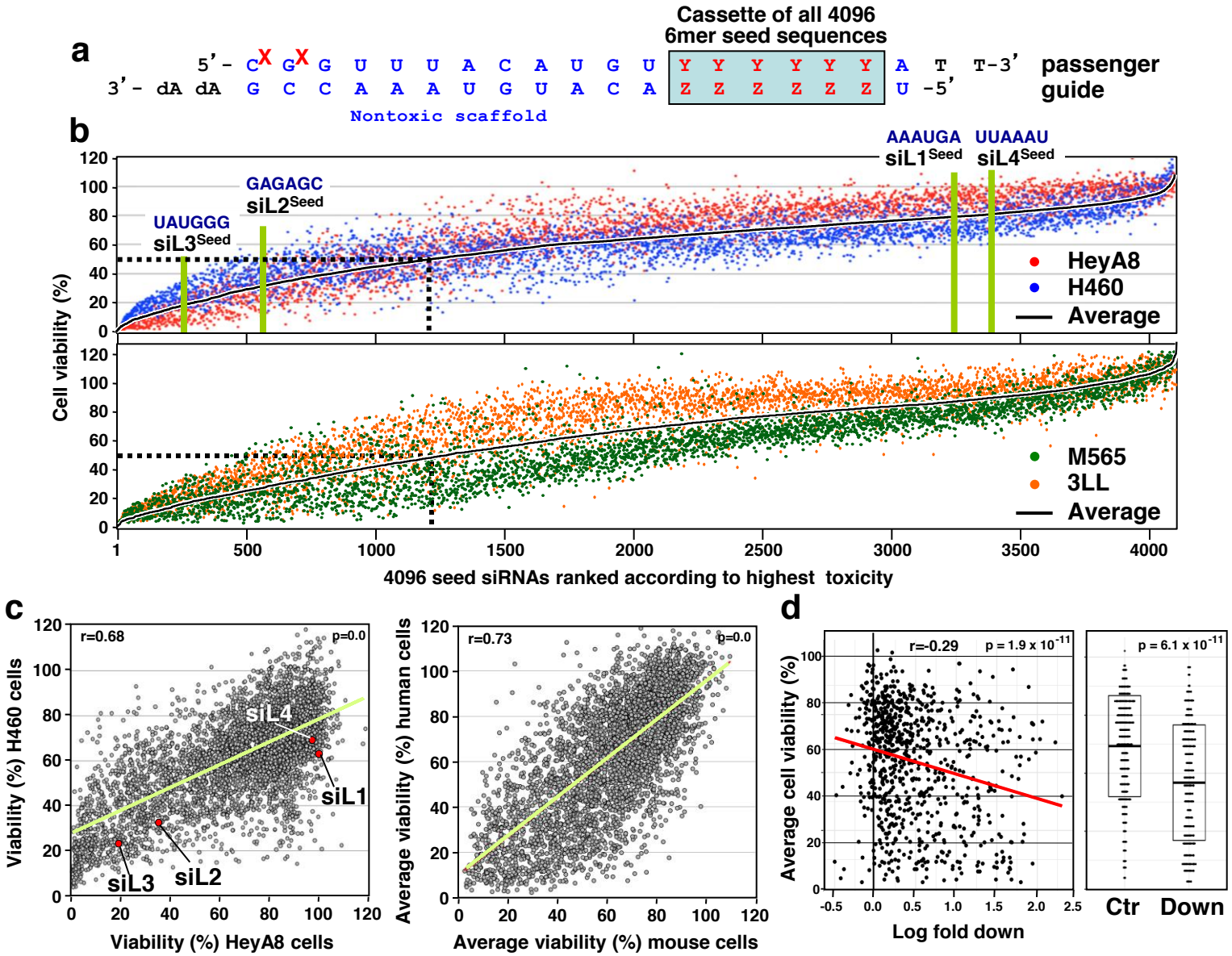
a
Cassette of all 4096
6mer seed sequences
5'- C X G X G U U U A C A U G U Y Y Y Y Y Y A T T-3' passenger
3'- dA dA G C C A A A U G U A C A Z Z Z Z Z Z U -5' guide
Nontoxic scaffold
b
UAUGGG siL3Seed
GAGAGC siL2Seed
AAAUGA siL1Seed
UUAAAU siL4Seed
HeyA8
H460
Average
M565
3LL
Average
Cell viability (%)
4096 seed siRNAs ranked according to highest toxicity
c
r=0.68
p=0.0
siL4
siL1
siL3
siL2
Viability (%) H460 cells
Viability (%) HeyA8 cells
r=0.73
p=0.0
Average viability (%) human cells
Average viability (%) mouse cells
d
r=-0.29
p = 1.9 x 10-11
Average cell viability (%)
Log fold down
p = 6.1 x 10-11
Ctr
Down

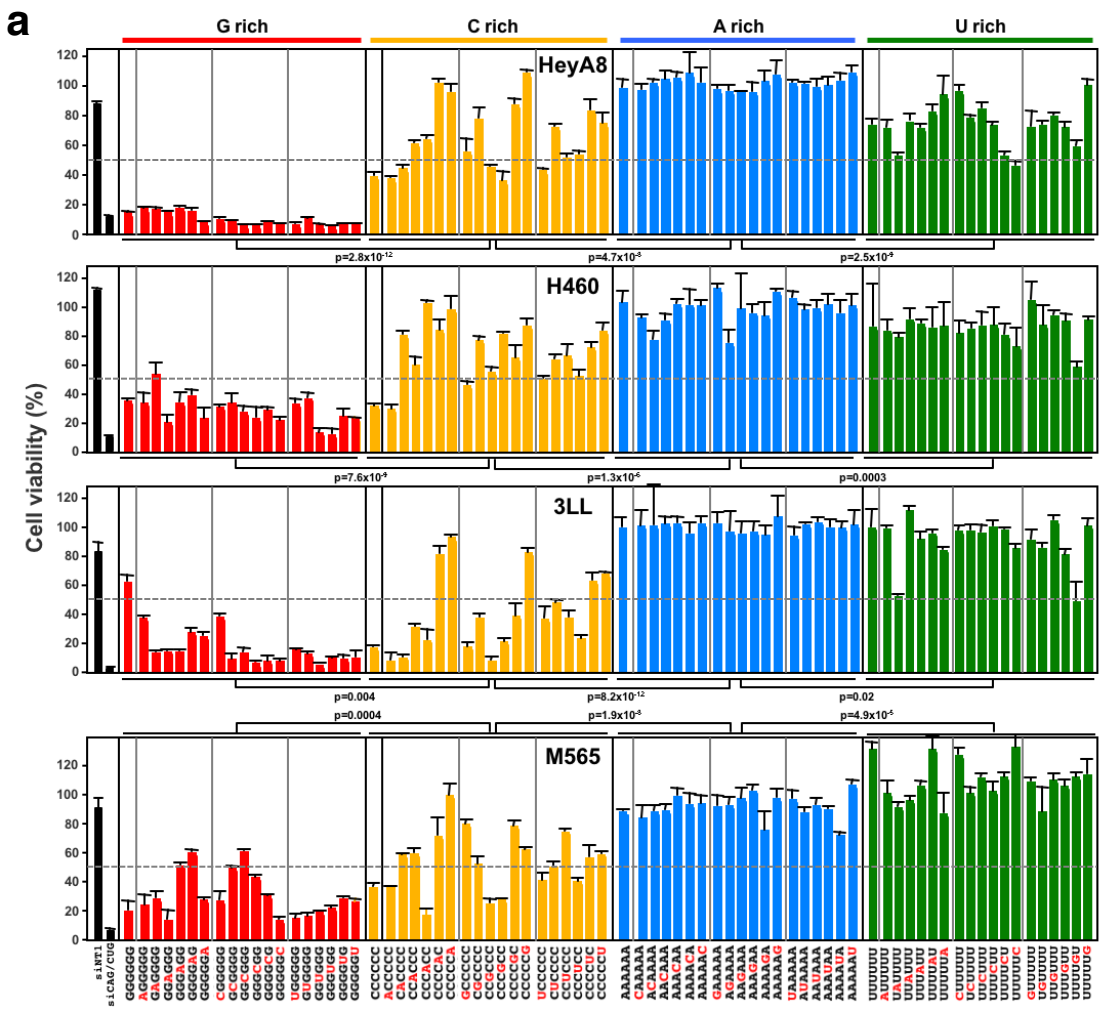
a
G rich
C rich
A rich
U rich
HeyA8
H460
3LL
M565
Cell viability (%)
p=2.8x10-12
p=4.7x10-5
p=2.5x10-9
p=7.6x10-4
p=1.3x10-6
p=0.0003
p=0.004
p=8.2x10-12
p=0.02
p=0.0004
p=1.9x10-3
p=4.9x10-5
siNT1
siCAG/CUG

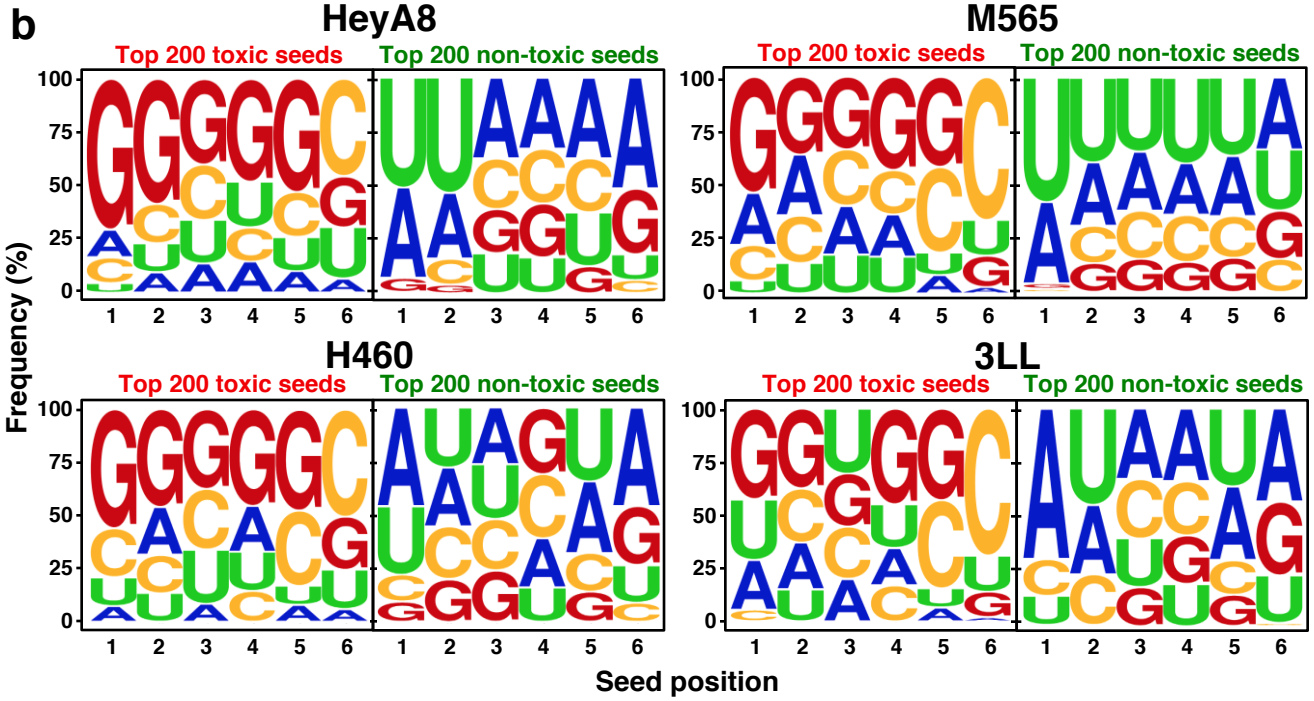
b
HeyA8
M565
H460
3LL
Top 200 toxic seeds
Top 200 non-toxic seeds
Frequency (%)
Seed position

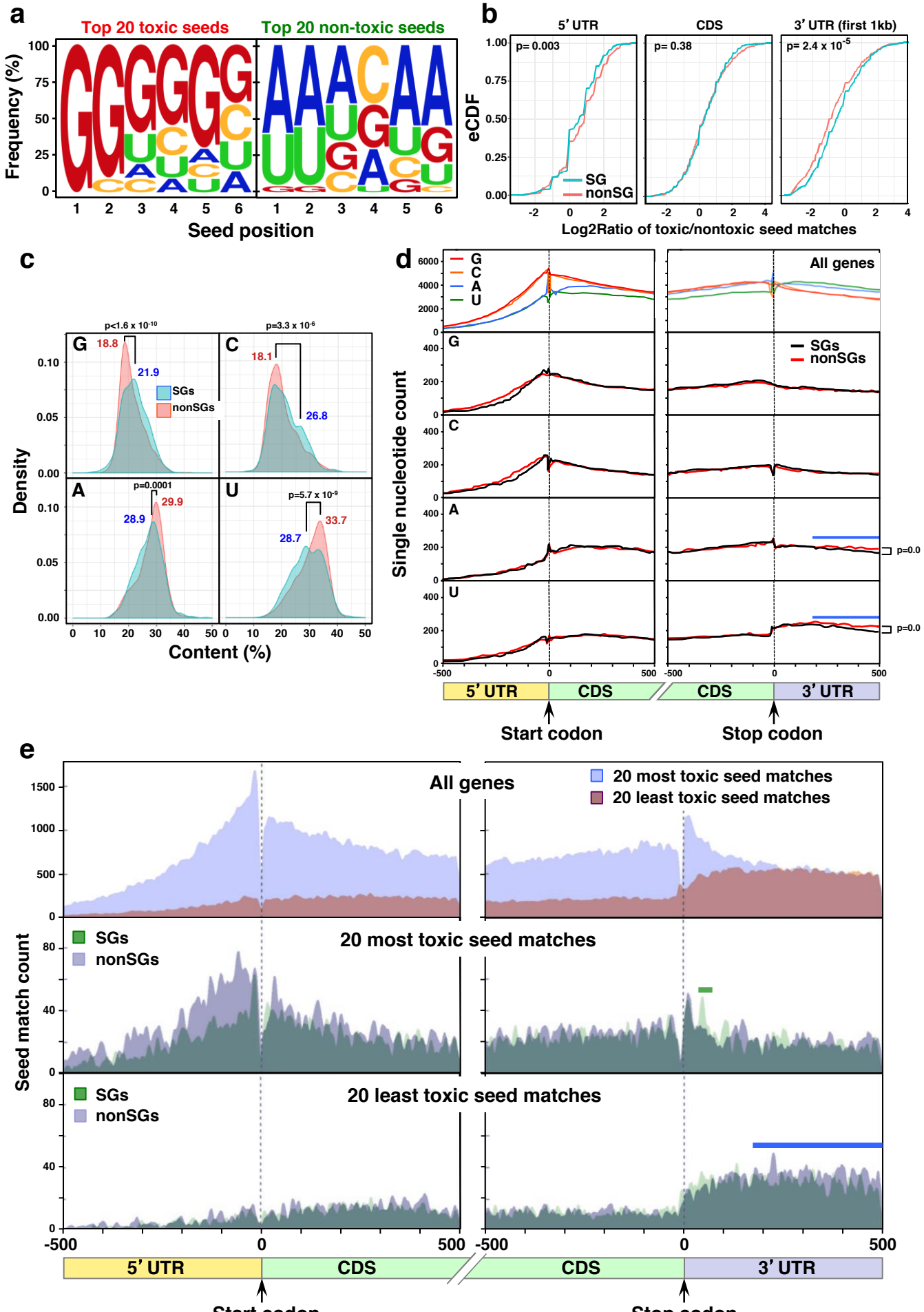

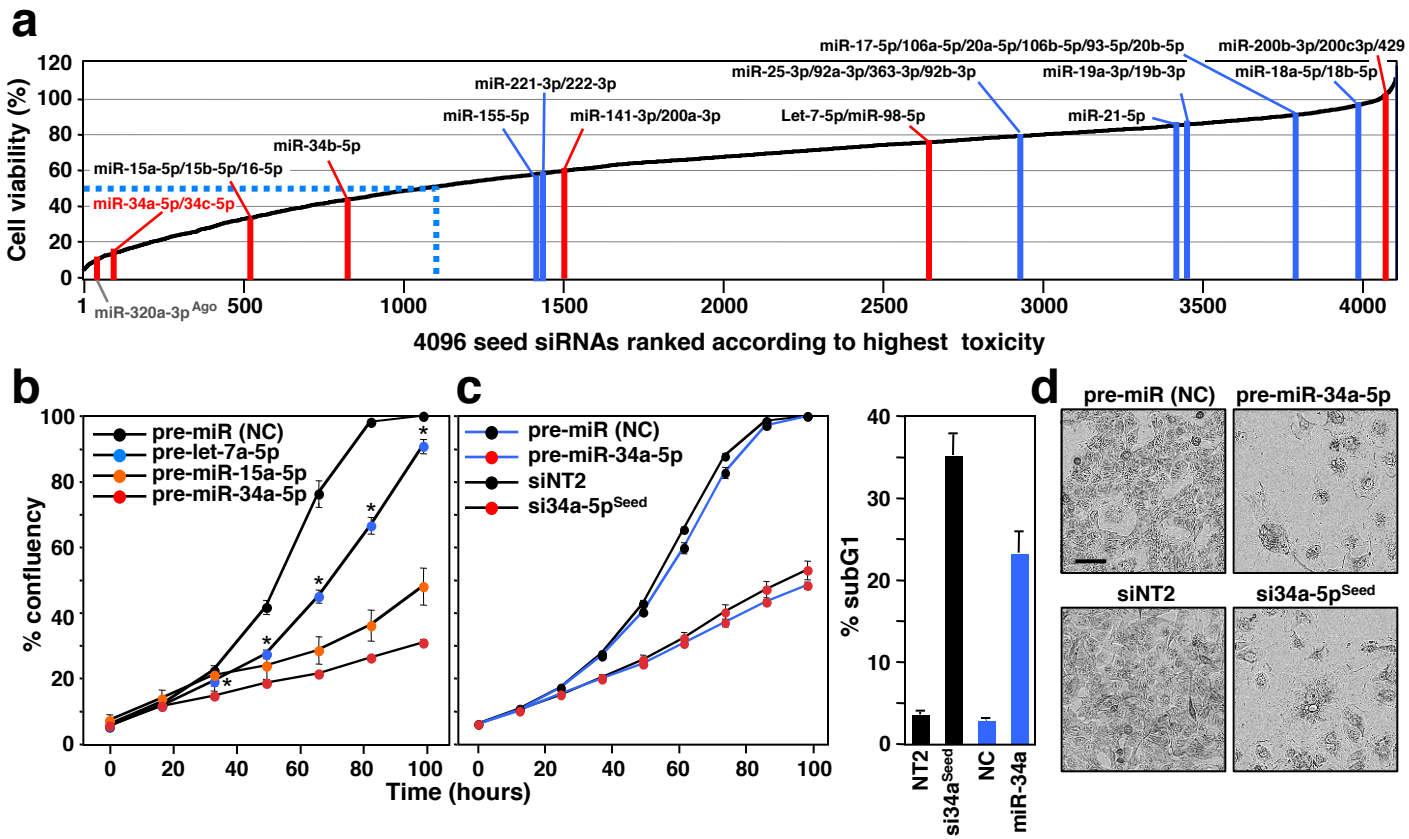
a
Cell viability (%)
miR-320a-3p Ago
miR-15a-5p/15b-5p/16-5p
miR-34a-5p/34c-5p
miR-34b-5p
miR-155-5p
miR-221-3p/222-3p
miR-141-3p/200a-3p
Let-7-5p/miR-98-5p
miR-25-3p/92a-3p/363-3p/92b-3p
miR-21-5p
miR-19a-3p/19b-3p
miR-17-5p/106a-5p/20a-5p/106b-5p/93-5p/20b-5p
miR-18a-5p/18b-5p
miR-200b-3p/200c3p/429
4096 seed siRNAs ranked according to highest toxicity
b
% confluency
pre-miR (NC)
pre-let-7a-5p
pre-miR-15a-5p
pre-miR-34a-5p
Time (hours)
c
pre-miR (NC)
pre-miR-34a-5p
siNT2
si34a-5pSeed
% subG1
NT2
si34aSeed
NC
miR-34a
d
pre-miR (NC)
pre-miR-34a-5p
siNT2
si34a-5pSeed

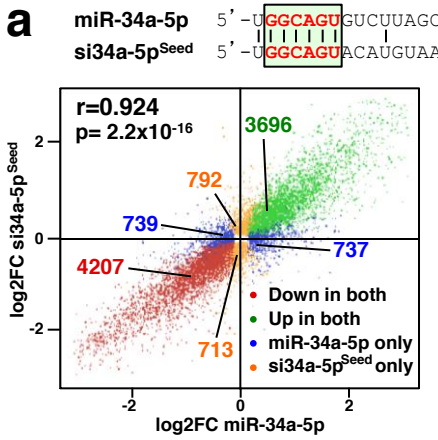

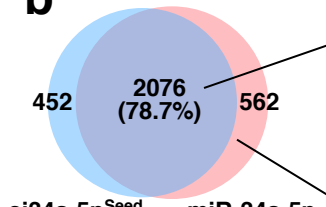

GO Term	Description	P-value	FDR q-value	Enrichment
GO:0022402	cell cycle process	3.25E-27	2.60E-23	2.0
GO:0065004	protein-DNA complex assembly	2.80E-23	1.12E-19	3.8
GO:0071824	protein-DNA complex subunit organization	6.06E-22	1.61E-18	3.6
GO:0006334	nucleosome assembly	3.38E-21	6.75E-18	3.9
GO:1903047	mitotic cell cycle process	8.37E-21	1.34E-17	2.0
GO:0034728	nucleosome organization	4.22E-20	5.62E-17	3.7
GO:0051276	chromosome organization	6.66E-19	7.59E-16	2.7
GO:0006325	chromatin organization	5.75E-16	5.74E-13	4.7
GO:0006342	chromatin silencing	5.37E-15	4.76E-12	4.3
GO:0045814	negative regulation of gene expression, epigenetic	1.16E-14	9.28E-12	4.1
GO:0016458	gene silencing	5.56E-13	4.03E-10	6.9
GO:0051301	cell division	7.46E-13	4.96E-10	2.0
GO:0038111	interleukin-7-mediated signaling pathway	1.64E-12	1.01E-09	19.3
GO:0000183	chromatin silencing at rDNA	3.29E-12	1.88E-09	5.3
GO:0006259	DNA metabolic process	4.15E-12	2.21E-09	1.5

GO Term	Description	P-value	FDR q-value	Enrichment
GO:0015718	monocarboxylic acid transport	4.59E-06	1.82E-02	22.5
GO:0006869	lipid transport	2.57E-05	5.09E-02	14.1
GO:0015850	organic hydroxy compound transport	1.02E-04	1.35E-01	22.5
GO:0015849	organic acid transport	1.83E-04	1.81E-01	6.0
GO:0046942	carboxylic acid transport	1.83E-04	1.45E-01	6.0
GO:0006820	anion transport	4.80E-04	3.17E-01	9.4

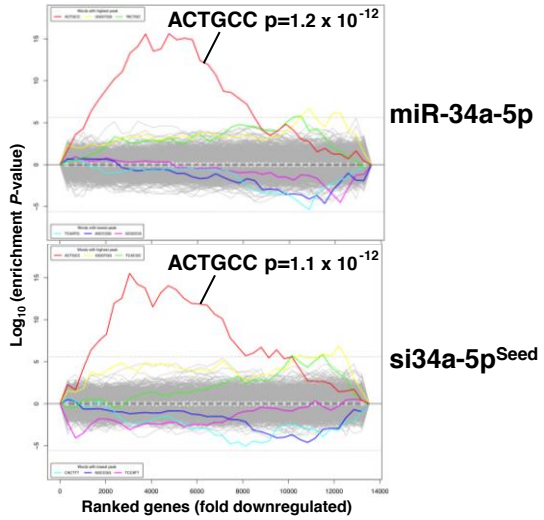

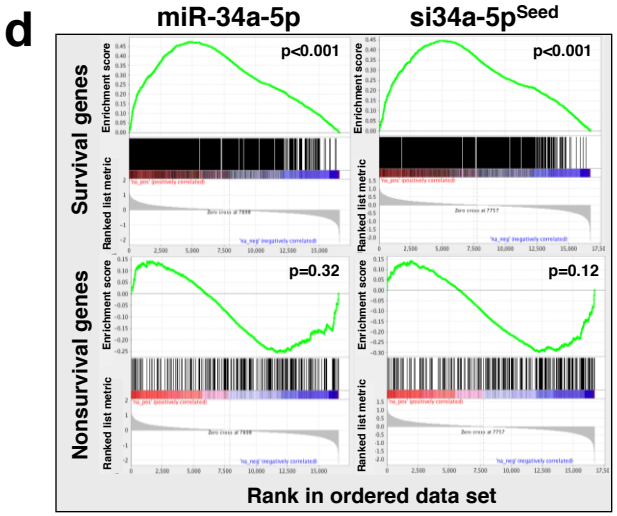

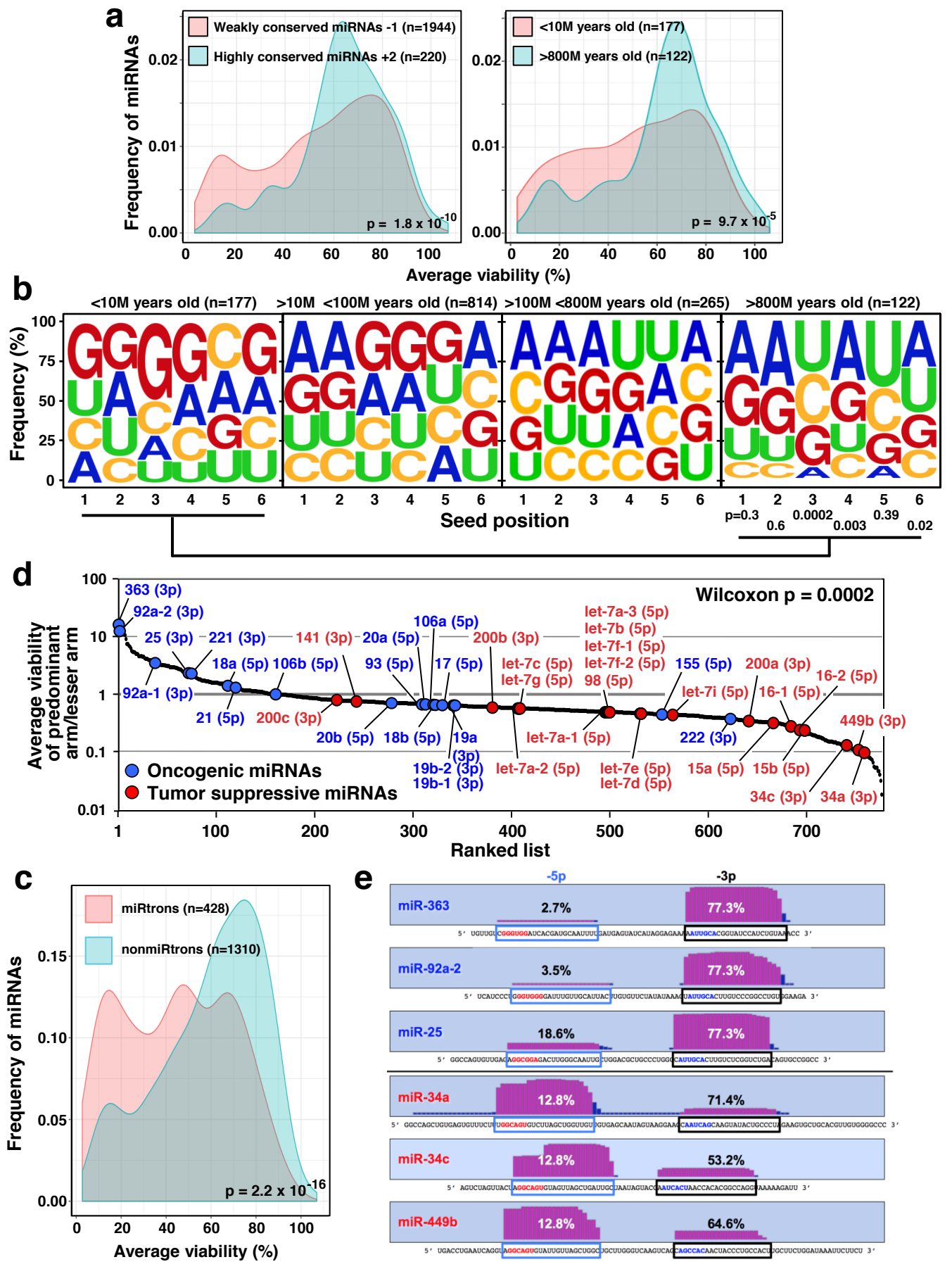
a
Weakly conserved miRNAs -1 (n=1944)
Highly conserved miRNAs +2 (n=220)
p = 1.8 x 10-10
<10M years old (n=177)
>800M years old (n=122)
p = 9.7 x 10-5
Frequency of miRNAs
Average viability (%)
b
<10M years old (n=177)
>10M <100M years old (n=814)
>100M <800M years old (n=265)
>800M years old (n=122)
Frequency (%)
Seed position
p=0.3
0.6
0.0002
0.003
0.39
0.02
d
Wilcoxon p = 0.0002
Average viability of predominant arm/lesser arm
Ranked list
Oncogenic miRNAs
Tumor suppressive miRNAs
363 (3p)
92a-2 (3p)
25 (3p)
221 (3p)
141 (3p)
20a (5p)
106a (5p)
200b (3p)
let-7a-3 (5p)
let-7b (5p)
let-7f-1 (5p)
18a (5p)
106b (5p)
93 (5p)
17 (5p)
let-7c (5p)
let-7g (5p)
let-7f-2 (5p)
98 (5p)
155 (5p)
200a (3p)
16-2 (5p)
92a-1 (3p)
let-7i (5p)
16-1 (5p)
21 (5p)
200c (3p)
449b (3p)
20b (5p)
18b (5p)
19a (3p)
let-7a-1 (5p)
222 (3p)
19b-2 (3p)
19b-1 (3p)
let-7a-2 (5p)
let-7e (5p)
let-7d (5p)
15a (5p)
15b (5p)
34c (3p)
34a (3p)
c
miRtrons (n=428)
nonmiRtrons (n=1310)
p = 2.2 x 10-16
Frequency of miRNAs
Average viability (%)
e
-5p
-3p
miR-363
2.7%
77.3%
miR-92a-2
3.5%
77.3%
miR-25
18.6%
77.3%
miR-34a
12.8%
71.4%
miR-34c
12.8%
53.2%
miR-449b
12.8%
64.6%

Figure 7

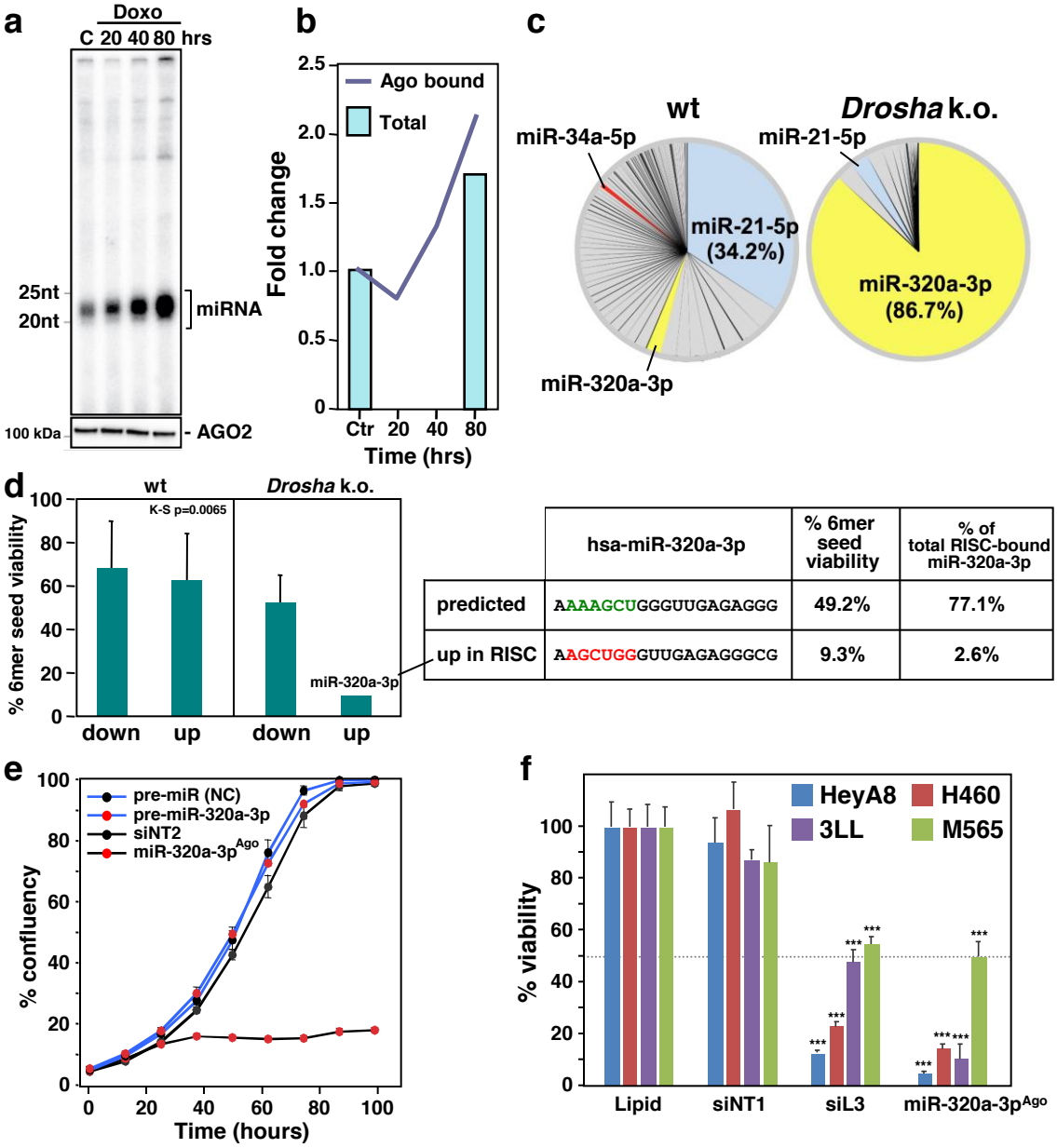

	hsa-miR-320a-3p	% 6mer seed viability	% of total RISC-bound miR-320a-3p
predicted	AAAAGCUGGGUUGAGAGGG	49.2%	77.1%
up in RISC	AAGCUGGGUUGAGAGGGCG	9.3%	2.6%